Journal of Materials Chemistry C

Harnessing biological applications of quantum materials: opportunities and precautions

Journal:	*Journal of Materials Chemistry C*
Manuscript ID	TC-HIG-05-2020-002429.R1
Article Type:	Highlight
Date Submitted by the Author:	02-Jul-2020
Complete List of Authors:	Modayil Korah, Mani; Arizona State University, Chemical Engineering Nori, Tejaswi; Arizona State University, Chemical Engineering Tongay, Sefaattin; Arizona State University, Materials Science and Engineering Green, Matthew; Arizona State University, Chemical Engineering

Harnessing biological applications of quantum materials: Opportunities and precautions

Received 00th January 20xx,
Accepted 00th January 20xx

DOI: 10.1039/x0xx00000x

Mani Modayil Korah,[a] Tejaswi Nori,[a] Sefaattin Tongay[b] and Matthew D. Green*[a]

Since the discovery of graphene, research on two-dimensional (2D) quantum materials has generated a plethora of novel materials with the potential to significantly change our lives. Owing to their unique quantum, electronic, and excitonic properties, biosensing and bio-imaging are two specific areas where these quantum materials have started to make a large impact. This article provides a holistic overview into the properties, synthesis methods, biological applications, and toxicology studies of commonly studied quantum materials. Recent research into the biological applications of graphene and transition metal dichalcogenides is highlighted and their unique electronic properties are explored. Though tremendous research is generated in discovering new 2D materials, toxicology studies in the area is lacking. Historically, toxicology studies have lagged significantly behind new material discovery often with dire consequences. The product development cycle of polymeric materials is a testament to the negative consequences of having a reactionary approach to toxicology. With 2D materials set to become a widespread part of everyday life in the near future, we comment on the need for a proactive approach to examining and understanding their toxicology.

1 INTRODUCTION

From the isolation and characterization of graphene by Geim and Novoselov[1] in 2004, interest in 2D materials for various applications has been on the rise owing to their unique electronic, optical, and magnetic properties. The growing scientific interest in 2D materials is driven by the extraordinary quantum properties realized in these materials which cannot be accessed in traditional systems. This coupled with the increasing demand to miniaturize electronics for applications in nanotechnology and microelectronics for the Internet of things, portable bioelectronics for biosensing and bioimaging **(Figure 1)** , and quantum computing[8] naturally positioned 2D crystals at the forefront of active research and engineering. Here, 2D materials or 2D quantum materials are defined as materials that are single unit cell thick (a single atom, or a few atoms, thick) sheets with lateral dimensions ranging from a few µm to ~50 mm.

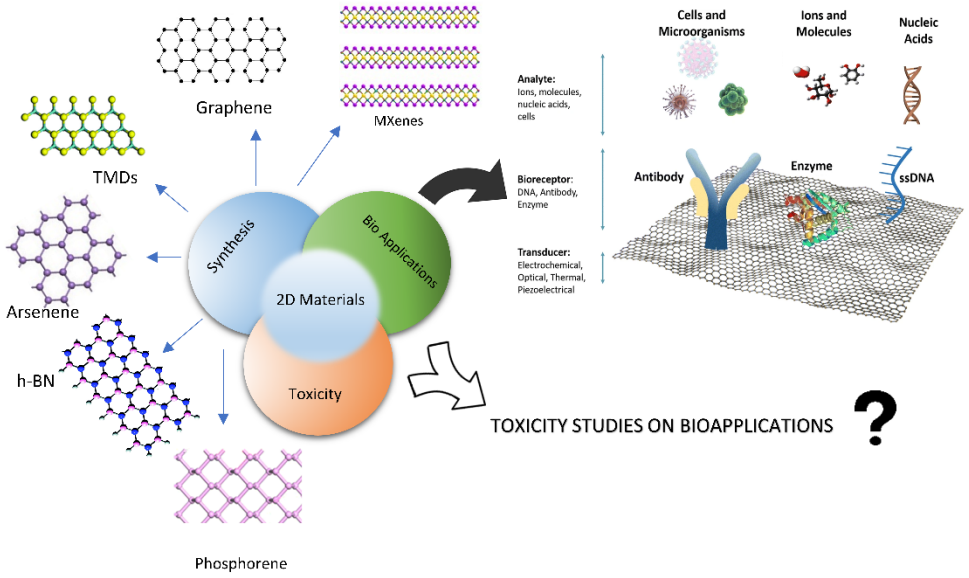

Figure 1 Overview of 2D Materials: Biological applications of 2D materials and the gaps between studies in the biological applications of 2D materials and the toxicity of 2D materials. Examples of biosensors and components on a graphene platform, adapted from ref. [34], licenced under CC by 4.0 . MXenes structure modified with permission from ref. [4]. Copyright 2019, Elsevier. Graphene structure modified from ref. [2], licenced under CC by 3.0. TMDs structure adapted from Ref. 3 with permission from The Royal Society of Chemistry. Arsenene structure modified with permission from ref. [5]. Copyright 2015, Elsevier. h-BN structure adapted from Ref. 6 with permission from The Royal Society of Chemistry. Phosphorene structure adapted from with permission from ref. [7]. Copyright (2015) American Chemical Society

[a] *Department of Chemical Engineering, School for Engineering of Matter, Transport and Energy, Arizona State University, Tempe, AZ 85287, USA*
[b] *Department of Materials Science and Engineering, School for Engineering of Matter, Transport and Energy, Arizona State University, Tempe, AZ 85287, USA.*
*Corresponding author.
E-mail address: mdgreen8@asu.edu
† Footnotes relating to the title and/or authors should appear here.
Electronic Supplementary Information (ESI) available: [details of any supplementary information available should be included here]. See DOI: 10.1039/x0xx00000x

The synthesis of graphene by Geim and Novoselov[1] opened new areas of research in the fields of chemistry and physics. Graphene's extremely high room-temperature carrier mobility, specific area, Young's modulus, optical transparency, and excellent thermal and electrical conductivities have made it a point of research since 2004.[1,9–12] These unusual properties of graphene can be attributed to quantum confinement of the electrons in graphene.[13]

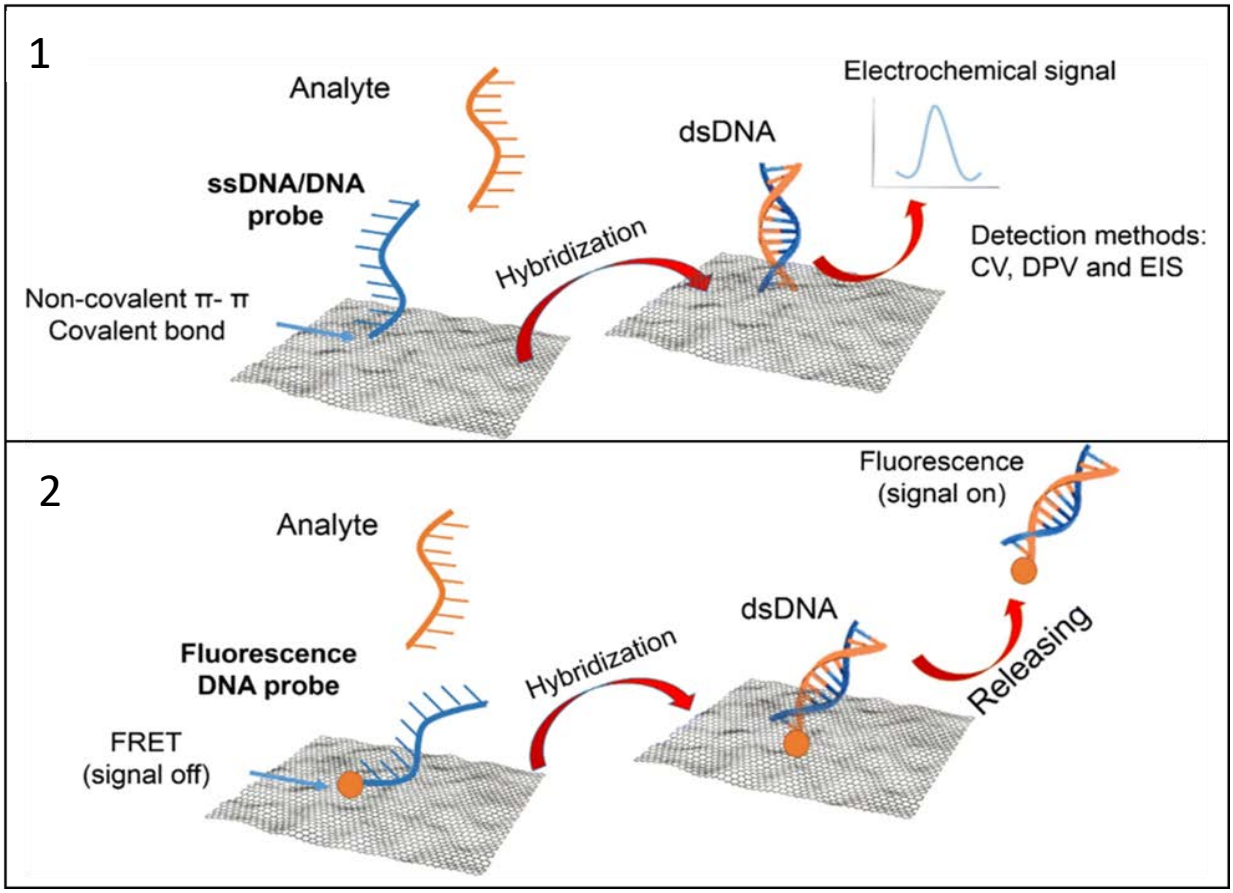

Figure 2 Scheme of Graphene-based nanomaterials as biosensors, Adapted from ref. [34], licenced under CC by 4.0 with changes in captions (from letter-based caption to roman numerals-based caption) 1) Biosensor based on electrochemical detection 2) Biosensor based on Forster Resonance Energy Transfer (FRET) fluorescence detection.

Since the discovery of graphene, research into other 2D materials such as transition metal dichalcogenides (TMDs),[14] transition metal oxides (TMOs),[15] hexagonal-boron nitride (h-BN),[16] MXenes [17] (metal carbides and metal nitrides where M is the metal atom and X is the carbon or nitrogen atom), metal organic frameworks (MOFs),[18] and analogs of graphene[19] such as black phosphorous (phosphorene), antimonene, arsenene, etc. has increased, revealing much about their properties. In addition to these, a completely new class of atomically thin materials have emerged with extraordinary quantum properties and effects that cannot be easily explained within established quantum mechanical theories. Examples include topological insulators,[20] Weyl fermions,[21] and excitonic insulators.[22]

The unique properties of 2D materials have enabled their use in different fields, ranging from electronic to biomedical applications. Since most of the 2D materials have tunable bandgaps in the ranges of visible light wavelengths,[23] near-infrared wavelengths,[24] and all the way to the long-wavelength infrared wavelengths,[25] they immediately found a use in a wide range of optoelectronic devices such as photodetectors.[26] The electronic properties of 2D materials range from being insulators,[27] to semiconductors,[28] to conductors,[29] because of which they find use in a wide range of electronic applications like Field-Effect Transistors (FETs).[30–32] For example, 2D WS_2 has been used as a biosensing platform to detect biomarkers such as microRNA,[33] due to its abilities to quench fluorescence and mimic some enzyme functions.

Biosensors are devices which convert biological responses or biomolecules of interest in the target into readable electronic or optical signals. A biosensor typically consists of the active element, which is the part that senses the target molecules, an electronic transducer to convert the biochemical response into an electrochemical, optical or an electronic signal, and a signal amplifier.[34] The active element in a biosensor usually contains probe molecules which give out an electrochemical or optical response which is captured by the transducer. **Figure 2** shows the schematic of a typical graphene based active element with two types of biochemical responses: 1) an electrochemical signal and 2) Förster Resonance Energy Transfer (FRET) fluorescence. Some 2D materials, such as graphene and TMDs, have been shown to be biocompatible and have a high charge carrier density, hence, are a good choice as

the sensing element in the biosensors.

Although 2D materials find use in a wide array of applications, there are still significant challenges that hinder the complete commercialization of these materials. Challenges like scalability, cost effectiveness, lack of precise control over structure and surface functionalization, and reproducibility are still limiting commercialization and widespread use of these materials.[35,36] Moreover, there is a very significant and obvious lag in the research to determine the biocompatibility and toxicity of these 2D materials. In spite of these challenges, there has been a rapid increase in the research undertaken to explore the properties and applications of 2D materials in areas like biosensing and bioimaging. Therefore, elucidating the inadvertent effects that this unique class of material could have on cells and organisms with which it will interact is crucial prior to its implementation in biomedical applications. Furthermore, the figure-of-merit or standard method(s) to assess the biocompatibility of 2D materials is not well-established in the field. This article highlights recent work that studied the biological applications of several 2D materials, spotlights several promising applications for the future, and reviews the limited toxicology information available for 2D materials.

1.1 Properties of 2D materials:

2D materials have interesting properties which differ greatly from their bulk 3D counterparts, such as tuneable band gaps, high carrier mobility and mechanical properties such as high tensile strength. These properties are highly desired in applications like optoelectronics, semiconductors and in biosensors. In this section, we will be highlighting the properties of some of the popular 2D materials.

1.1.1 Graphene

Graphene has a room-temperature electron mobility of 2.5 x 10^5 cm^2 V^{-1} s^{-1}, [37] an intrinsic strength of 42 N m^{-1} and a 3D Young's modulus of 1 TPa.[10] The intrinsic strength is defined as the maximum stress that can be supported by a defect-free, pristine material prior to failure. The intrinsic strength measurement was first obtained by Lee *et al.* and is related to the strength of the atomic bonds rather than sizes of defects and flaws within the material.[10] It is important to note that the 3D Young's modulus is obtained from 2D Young's modulus measurements by assuming a thickness (h) of 0.335 nm (Y_{3D} = Y_{2D}/h). However, the behaviour of true 2D materials like monolayer graphene under tensile loading is described by 2D stress and 2D elastic constants with units of N m^{-1}. These 2D parameters scale with the planar elastic energy as opposed to volumetric elastic energy in 3D materials.[10,38] The conversion to 3D material properties for 2D materials is done for purposes of comparison to bulk materials.

It has an extremely low permeability to all gases[39] and can have a wide variety of surface functionalization groups that can be tailored for a given application.[40,41] These properties of graphene enable it to be used for applications in a variety of fields. For example, graphene has an optical transmittance of 97.7% per layer,[11] allowing it to be used as a transparent conductive coating in touchscreen displays and organic LEDs. Graphene, although slightly inferior to indium tin oxide (ITO) in conductive characteristics, is considerably cheaper than ITO and has the added advantage of being extremely flexible and durable. Specifically, graphene has a fracture strain about ten times higher than ITO and a uniform absorption across the visible spectrum, which gives graphene an edge over ITO and enables it to be used in roll-to-roll processing and bendable electronics.[10,42]

The optical and conductive properties of graphene enable more than its implementation in flexible electronics. The electron transfer between the electrode and the probe biomolecule in a biosensor defines its sensitivity. Thus, the high carrier mobility in graphene enables graphene-based biosensors and biomedical devices in which the detecting signal is an electrochemical signal (**Figure 2.1**).[43–46] In addition to the high electron transport property of graphene, its high specific surface area make it an ideal candidate for biosensors.[7,17]

1.1.2Transition Metal Dichalcogenides (TMDs):

Transition metal dichalcogenides are materials with a stoichiometry of MX_2 (where M = a metal atom, typically Mo, Nb, Re, W, or Ni and X = a chalcogen atom, typically S, Se, or Te).[48] TMD crystals are layered materials with van der Waals forces across the adjacent layers wherein each individual 2D sheet is held together through strong covalent bonds. TMDs are of interest in the fields of electronics and optics due to the indirect to direct gap crossover going from bulk (indirect) to monolayers (direct).[49,50] This band renormalization can be attributed to quantum confinement of the electrons in the 2D limit. As the thickness of the MoS_2 layers decreases, the indirect band gap blue shifts from 1.3 eV in the bulk to 2.0 eV in the monolayer form.[51] Owing to their single unit cell thickness (0.7 nm), 2D MoS_2 and other TMDs -such as WSe_2 and $MoTe_2$- can be easily gated to create highly energy efficient field-effect transistors (FETs).[52]

Furthermore, 2D Mo- and W-containing TMDs (e.g., $MoSe_2$, WSe_2, etc.) have been shown to have large excitonic binding energies reaching world-record 0.4 eV values depending on the material systems.[53,54] This enabled researchers to access excitons at room temperature which was not possible prior to the discovery of 2D TMDs.[55,56] Later studies have further shown that these excitons can be accessed at different momentum (valley) points with spin information encoded.[57,58] This has created a new "valleytronics" field with a special emphasis on excitonic and optical applications.[59,60]

It is also noteworthy to mention that 2D TMDs have different crystalline phases depending upon the molecular arrangements. TMDs can exist in anisotropic 1T',[61] 1T (Trigonal),[62] 2H (Hexagonal),[63] or 3R (Rhombohedral)[64] phases where the metal coordination in the layers is either trigonal prismatic or octahedral. The filling of the d-orbitals in these compounds determines the

nature of the compound: partially filled d-orbitals give rise to metallic character whereas fully filled d-orbitals lead to semiconductor-like behaviour.[65,66]

It has been reported that the photoluminescence of MoS_2 increases by a factor of ~10^4 as the material thickness decreases from bulk to monolayer TMDs due to indirect to direct cross-over and high quantum efficiency associated with efficient exciton relaxation pathways.[67] Therefore, optical plasmonic sensors based on 2D TMDs have been predicted to have stronger responses when compared to sensors based on metallic substrates such as gold or silver.[68] TMDs have large surface areas and large interfacial contact areas between the materials and the electrodes, making it possible to have very strong interfacial interactions. Consequently, TMDs exhibit rapid interfacial charge transfer which translates to a highly accurate biosensing platform. Additionally, TMDs also have high biocompatibility which allows for the immobilization of different probe biomolecules onto the surface of the materials. Combined with high carrier density and rapid interfacial charge transfer, this amplifies the signals received from the biological phenomena being measured.[69] This amplification can be used as a detection mechanism for important biomolecules present at very low concentrations, which are otherwise extremely difficult to detect using current state-of-the-art methods such as enzyme-linked immunosorbent assay (ELISA) or polymerase chain reaction (PCR).

1.1.3 Transition Metal Oxides:

Transition Metal Oxides (TMOs), in their bulk form have been studied extensively; however, 2D TMOs are difficult to fabricate, which has limited the investigation of 2D TMOs in literature.[70] Due to the polarizability of the oxygen ion and the hybridization of the orbitals, when two or more TMO layers are stacked, a potential arises between the sheets that shifts the Fermi levels of the layers and gives the layers semiconducting properties.[71,72] TMOs can be engineered to have a wide range of band gaps, depending on their applications in optoelectronics and semiconductors.[73,74] Semiconducting TMOs can be used to manufacture FETs, which have been implemented as memory and storage elements and in biosensors. FETs based on 2D TMOs, such as MoO_3, have been used as the sensing electrodes in biosensors due to their high electron mobility, which allows for the detection of biomolecules at low concentrations.[75]

2D TMOs have strong d-d transitions, which result in strong light absorption and allow them to quench luminescence via Forster Resonance Energy Transfer (FRET) when conjugated with fluorophores.[76] As a result, TMOs, such as MnO_2, have been used for fluorescence imaging of glutathione, which is a biomarker used to detect cancer cells.[77]

1.1.4 MXenes:

MXenes are a class of 2D materials with a stoichiometry of $M_{n+1}X_n$ (n = 1, 2, or 3) where M is a transition metal and X is either a carbon or nitrogen. They are synthesized by etching the MAX phases, which have a stoichiometry of $M_{n+1}AX_n$ (where A is a IIIA or IVA group element), with HF.[78] MXenes have reported Young's moduli in the range of 92 to 161 N m^{-1}, comparable to that of TMDs.[79] Some MAX phases, such as Ti_3AlC_2, have a very high resistance to oxidation which enables their utilization as high-temperature electromagnetic sensors.[80] MXenes also exhibit high enzyme immobilization capabilities and are compatible with redox proteins, with high bioactivity, making them possible candidates to build electrochemical biosensors.[81]

1.1.5 Metal Organic Frameworks:

MOFs are porous materials which are synthesized by linking metal ions to organic ligands to form a coordinated and layered structure. MOFs have tunable structures, are highly porous, and have a very high surface area.[82] MOFs have tunable bandgaps which can be adjusted by changing the metal ions and the organic ligands, ranging from Cu, Zn-based insulator MOFs to Cu, Zn-tetrakis(4-carboxyphenyl)porphyrin (TCPP)-based MOFs which are semiconducting in nature. The high porosity, high surface area, and the tunability of the structures allow MOFs to be used in various applications. The high porosity and surface area were exploited by Yan *et al*. in synthesizing a porous C/ZnO nanocomposite 2D semiconductor based on fluorinated-MOFs (F-MOFs) with a porosity of 732 m^2 g^{-1} and a high electrical conductivity of 43 S m^{-1}. [83]

1.1.6 Analogs of Graphene:

Other graphene-like materials such as silicene,[84,85] graphitic-carbon nitride (g-C_3N_4),[86,87] hexagonal- Boron Nitride (h-BN),[88] and 2D pnictogens such as phosphorene,[89,90] antimonene,[91,92] and arsenene[93,94] have also been researched for applications in various fields, including semiconductors and biosensors. Silicene is a direct bandgap semiconductor with a bandgap of 210 meV and a carrier mobility of 100 cm^2 V^{-1} s^{-1}.[85] Hexagonal boron nitride is an indirect wide-bandgap semiconductor which finds use in different types of nanoelectronics and optoelectronics.[95] Hexagonal boron nitride has a Young's modulus of 780 GPa, a very high surface area (1427 m^2 g^{-1}) and is also biocompatible which allow for biological applications like drug delivery, nanomedicine and biosensors.[96–99] Black phosphorus, or phosphorene, has a direct band gap of ~2 eV at the single layer level and high carrier mobility of 1.5×10^4 cm^2 V^{-1} s^{-1} at 294 K, making it a suitable material for optoelectronics.[100] The unique surface morphology of phosphorene allows for the immobilization of various probe biomolecules, such as single-stranded DNA (ssDNA), onto the surface to serve as biosensors.[101] Mayorga-Martinez *et al*. reported a pnictogen-based enzymatic phenol biosensor, where it was found that heavier pnictogen-based 2D materials, such as antimonene and bismuthine, had higher stabilities than phosphorene.[94] The group tested enzymatic biosensors based on phosphorene, arsenene, antimonene, and bismuthine and it was found that the antimonene-based biosensor showed enhanced selectivity, reproducibility, and sensitivity with a limit of detection of 2.5×10^5 pM.

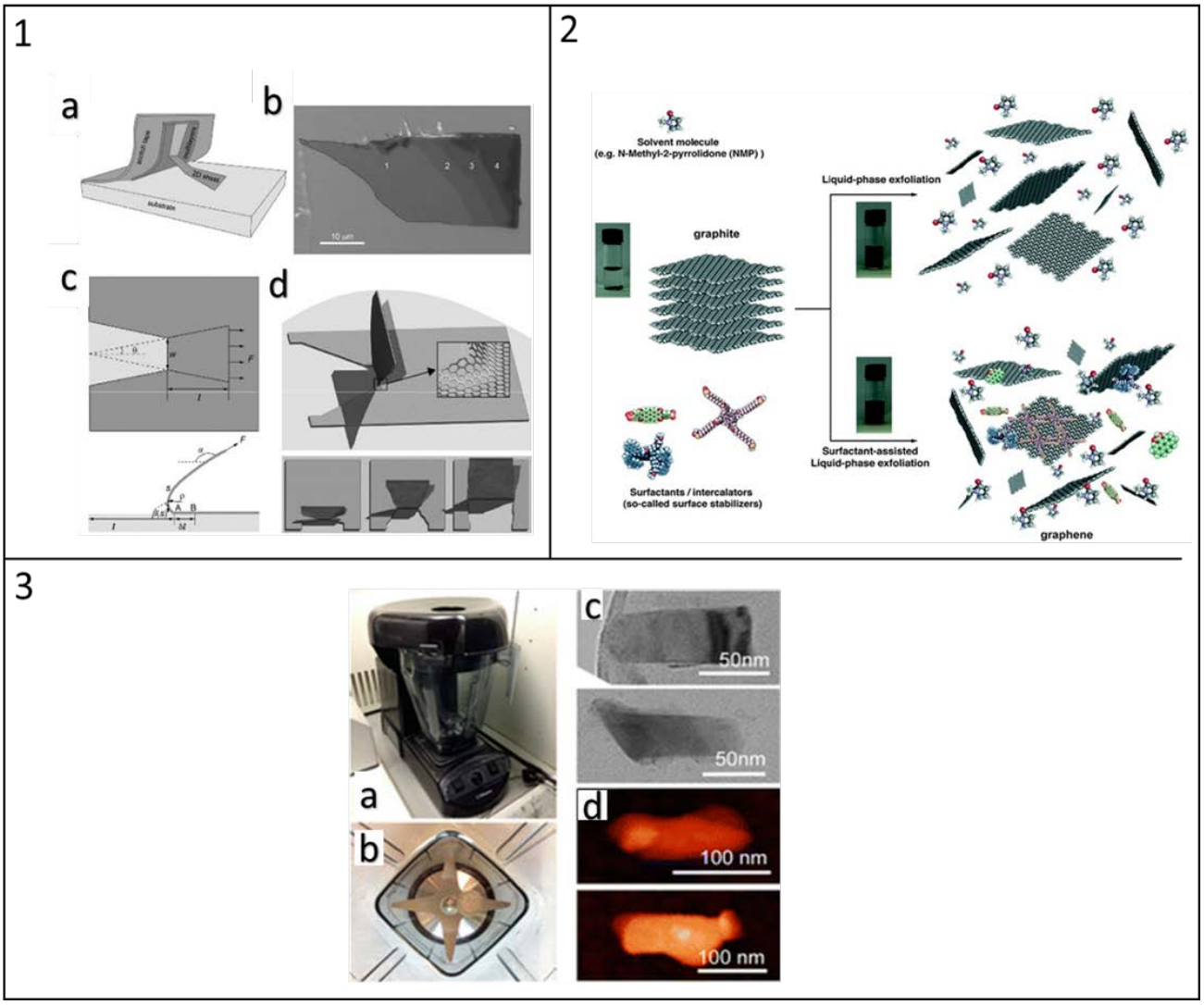

Figure 3 Top-down approaches for 2D materials synthesis: i) micromechanical cleavage: 1-a) Schematic illustration of mechanical cleavage with an adhesive tape 1-b) Optical Image of exfoliated graphene with the number of layers being denoted by the numbers 1-c) Top and side views of a 2D sheet being peeled off 1-d) Detailed view of the front and edges of the 2D sheet being peeled off, obtained from course-grained molecular dynamics simulations. Reproduced with permission from ref. [103]. Copyright 2018, Elsevier 2) sonication-assisted liquid exfoliation. Ref. [111] Reproduced by permission of The Royal Society of Chemistry 3) shear force-assisted liquid exfoliation. Adapted with permission from ref. [114]. Copyright (2015) American Chemical Society : 3-a)mixer used for shear force-assisted exfoliation, 3-b) blade assembly shown with €2 coin for scale, 3-c) TEM images of flakes produced with shear force-assisted exfoliation, 3-d) AFM images of flakes produced with shear force-assisted-exfoliation

2 SYNTHESIS

The properties of 2D materials depend upon their thickness, crystal phases, and surface properties. Therefore, synthesis methods that can control and tune these properties must be employed in the preparation of 2D materials. The synthesis of 2D materials can be broken down into two approaches: the top-down approach and the bottom-up approach. The top-down approach uses materials whose bulk crystals are layered materials held together by van der Waals forces. The bottom-up approach involves the reaction and/or deposition of the precursor molecules of the 2D material onto a substrate using different methods.[102] Both the top-down and the bottom-up approaches are briefly discussed below.

2.1 Top-down Synthesis of 2D Materials:

2.1.1 Micromechanical Cleavage:

This method involves mechanically removing layers of the bulk crystal using two adhesive layers. The method was first used by Geim and Novoselov[1] to synthesize atomically thin layers of graphene. In this process, the bulk material is first attached to Scotch™ tape, which is then peeled off into thin flakes using another piece of adhesive. This last step is repeated multiple times and then the adhesive tapes are attached to a clean, flat surface, usually glass, and rubbed to achieve further cleaving (**Figure 3.1**).[103] Materials with a single atomic layer or a thickness of a few layers are then obtained on the substrate by peeling off the Scotch™ tape from the substrate. This method can be applied to the synthesis of other families of 2D

materials such as TMDs,[104–106] phosphorene,[100,107,108] antimonene[109] and h-BN,[16,110]

Although this method has the advantage of creating layers with high crystal quality and large lateral lengths, it has many other disadvantages, stopping it from being utilized for the mass production of 2D materials. Specifically, this approach has a low production rate and yield, and leads to uneven thickness over the total surface created. These disadvantages arise due to this technique being hand driven, which introduces human error and reduces reproducibility and precision.

2.1.2 Mechanical force-assisted liquid exfoliation:

Mechanical force-assisted liquid exfoliation involves applying force on the layered bulk materials that are dispersed in liquid media. The mechanical force can be applied by either sonication[111,112] or by inducing mechanical shear[113,114] through high rpm mixing. Mechanical force-assisted liquid exfoliation has high yields when compared with other mechanical exfoliation techniques, like the Scotch™ tape method. These techniques can be used to produce large quantities of layered materials at low costs due to its simplicity. Although these techniques have advantages such as high yield and low costs of operation, one of the disadvantages of these techniques is the low yield of single layer nanosheets and limited lateral sizes. Some specific applications, such as semiconductor materials, require single layer nanosheets, which cannot be produced with enough quality control by this technique. Additionally, this process introduces a substantial amount of point or cluster defects, which adversely affects their much desired electronic, excitonic, and optical properties.

2.1.2a Sonication-assisted liquid exfoliation:

In a typical sonication-assisted liquid exfoliation, the bulk material is dispersed in a solvent, usually N-methylpyrrolidone.[104] Sonication induces liquid cavitation, which in turn creates bubbles. When these bubbles pop, it creates microjets and shockwaves between the layers of the bulk material, stripping thin layers or monolayers off (**Figure 3.2**). Although this method can produce layers ranging from one atom thickness to a thickness of a few layers at concentrations down to 1 mg mL^{-1} of the bulk material, it has a very slow production rate. For proper exfoliation to occur, the solvent and the bulk crystals must have the same surface energy, making it hard to find proper solvents. To overcome this, surfactants or polymers are added to tune the surface energy.[111]

The first use of this method was to synthesize graphene by Coleman and coworkers,[115] and since then the technique has been extended to other layered materials like MoS_2, WS_2, $MoSe_2$, $NbSe_2$, $MoTe_2$, h-BN.[116] TMOs such as MnO_2, TaO_3, Ti_4O_9 etc have also been exfoliated using this method.[73] The solvent chosen for the synthesis plays an important role in the exfoliation process: it was suggested that successful solvents for this process are the solvents which minimize the surface energy of the layers.[116] Different surfactants, such as cetyltrimethylammonium bromide,[117] sodium deoxycholate,[118] and polymers like poly(vinyl chloride), poly(methyl methacrylate), and poly(vinyl pyrrolidone), can also be added to the solution to decrease the surface energy.[119,120]

2.1.2b Shear Force-assisted Liquid Exfoliation:

In this method, the solution is mixed using a high shear rotor-stator mixer which produces high shear rates in the liquid under high speed rotation (**Figure 3.3**). The exfoliation of the layered bulk material is achieved by the high shear induced in the solvent by the rotors. The exfoliation only takes place if the shear rate is higher than 10^4 s^{-1}. Coleman and coworkers synthesized graphene using N-methylpyrrolidone as the solvent by subjecting it to shear mixing with a laboratory scale rotor-stator mixer. The final yield contained graphene layers ranging from monolayer thickness to thicknesses ranging from 300–800 nm; the typical thickness was 10 monolayers per sheet.[113] Varrla *et al*. synthesized 2D MoS_2 using this method obtaining layers with an average thickness of 5 layers and a mean sheet length of ~85 nm.[114]

Liu *et al*. investigated the factors influencing the final yield of the graphene synthesized by this method.[121] They reported that the effectiveness of exfoliation was influenced by the solution surface tension and viscosity. They also reported that the thickness and size of the nanosheets was controlled by the diameter of the rotor used. As in the case of sonication-assisted liquid exfoliation, surfactants and polymers can be used in shear force-assisted liquid exfoliation to increase the yield of the materials with single to multiple layers.

2.2 Bottom-up Synthesis of 2D Materials:

2.2.1 Chemical Vapor Deposition:

Chemical Vapor Deposition (CVD) is one of the most commonly used methods to synthesize 2D materials via the bottom-up approach, which yields thin films of highly pure materials.[122,123] In a typical process, substrates are placed in a chamber at variable pressure into which vapours of the precursor materials are sent. The precursor gases either react and then deposit onto the substrate, or the substrate is pre-treated with one of the precursors introduced in the chamber, onto which the second precursor reacts. Both pathways form ultrathin layers of the 2D material (**Figure 4.1**).[124] The factors that influence the deposition of the materials onto the substrate are the catalyst, temperature, substrate, precursors, and the atmosphere in which the reaction is taking place. CVD allows for precise control over the number of layers, lateral size, and crystallinity, each of which directly affect the optical and electronic properties of the grown material.[122,123,125–127]

Fu *et al*. synthesized graphene on a polycrystalline Ni substrate using CVD that was 1-2 layers thick over an area of 15,000 μm^2.[128] Other 2D materials such as ultrathin TMDs such as MoS_2, WS_2, $MoSe_2$;[127] 2D TMD hetero nanostructures, which are epitaxial

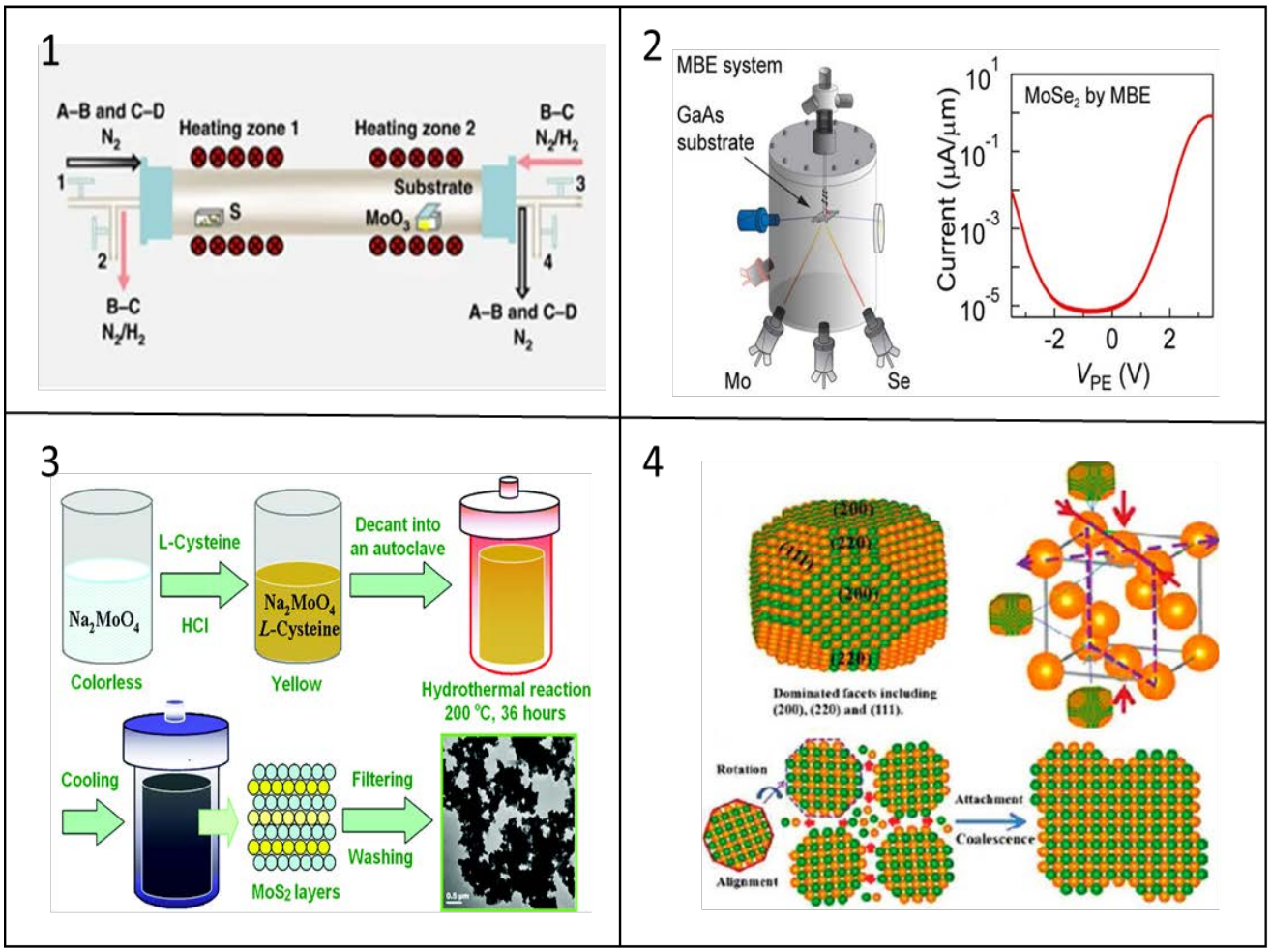

Figure 4 Bottom-up approach for 2D material synthesis: 1) Experimental setup of the modified sequential two-stage thermal CVD process , modified from Ref. [124], licenced under CC by 4.0 , 2) Schematic of Molecular Beam Epitaxy setup for the synthesis of MoS_2. Reproduced with permission from ref.[130]. Copyright (2017) American Chemical Society. Further permissions related to this material should be directed to ACS 3) Schematic of the hydrothermal synthesis technique. Reproduced from Ref. [141] with permission from The Royal Society of Chemistry 4) Self Assembly of nanocrystals. Adapted with permission from ref.[143]. Copyright (2011) American Chemical Society

structures with alternating layers of both of the TMDs[129] can also be grown on different kinds of substrates, making CVD one of the most versatile synthesis process currently available.

Although CVD has advantages such as high purity, limited defects, scalability and controllable thickness and extremely high yield, CVD operates at high temperatures and usually, under ultrahigh vacuum which adds up to a very high total cost of production.

2.2.2 Molecular Beam Epitaxy:

Molecular Beam Epitaxy (MBE) is a bottom-up synthesis technique for the epitaxial growth of controlled and advanced structures. The process takes place in an ultra-high vacuum chamber in which a substrate is heated to allow for epitaxial growth (**Figure 4.2**).[130] The ultra-pure precursors are placed in Knudsen cells, which sublime the precursors and shoot them out in a unidirectional beam of atoms or molecules onto the substrate. A separate Knudsen cell is used for each individual precursor. The flow of atoms or molecules onto the substrate builds up the layers of the material to be synthesized. A reflection high-energy electron diffraction (RHEED) system is used to monitor the epitaxial growth of the material on the substrate.[130]

Extremely precise control over the composition of the material grown, the growth conditions, and the purity of the material as well as *in situ* monitoring of the growth kinetics allow for highly complex and high quality materials to be synthesized using MBE.[131,132]

Although graphene is synthesized usually using techniques such as exfoliation or CVD, MBE can also be employed for the synthesis of graphene. Moreau *et al*. synthesized graphene via MBE using a heated graphite filament as the carbon source.[133] The graphene layer was epitaxially grown on a silicon carbide substrate to reduce lattice mismatches and produced two stacked layers that were 900 nm wide.

MBE can also be used for the synthesis of ultrathin TMDs, such as $MoSe_2$,[134] WSe_2,[135] and TMOs like VO_2[136] and $SrTiO_3$.[137] It is also used to synthesize 2D heterostructures that contain alternating

layers of two different 2D materials. Ma *et al*. synthesized a van der Waals heterostructure of $MoTe_2/MoS_2$.[138] MBE comes with its own disadvantages such as a slow growth rate, high complexity, and a high cost, even compared to CVD.

2.2.3 Wet Chemical Synthesis Techniques:

Wet chemical syntheses are bottom-up methods of synthesis involving chemical reactions for the formation of layered materials. These techniques have high yield and are highly reproducible.[112] Since the precursors involved in the reactions and the final layered materials are highly soluble in water and other organic solvents, these synthesis techniques are used to prepare 2D materials for a variety of applications. Techniques such as hydrothermal/solvothermal synthesis and nanocrystal self-assembly are discussed below.

2.2.3a Hydrothermal/Solvothermal Synthesis:

This method of synthesis involves the reaction of the precursors in either water or organic solvents under high temperatures and pressures.[139] The process is usually done in a sealed vessel at temperatures higher than the boiling point of the solvent, which increases the reaction pressure (**Figure 4.3**).[140] Parameters such as pH, temperature, pressure, additives (e.g., surfactants), concentration, and the reaction time can be varied to tune the properties of the layered materials.[141]

Dou *et al*. reported the synthesis of different TMOs such as TiO_2, ZnO, Co_3O_4, WO_3, Fe_2O_3, and MnO_2.[70] The thickness of the TMOs produced ranged from 1.6–5.2 nm, with a stacking of 2-7 layers. Chaudhary *et al*. reported the synthesis of MoS_2 nanosheets using hydrothermal synthesis. The synthesized sheets had a length of 100 nm and thicknesses up to 4 layers with a spacing of 0.68 nm in between the layers.[142]

These techniques are scalable techniques with simple setups when compared to other synthesis techniques such as CVD or MBE and have high yields. However, the growth mechanisms for these techniques are still not completely clear, which makes it difficult to model and design this method for different kinds of materials. This technique is also sensitive to the experimental conditions like the precursor concentration, solvent choice, the surfactants used, and the temperature of the reaction, which makes it difficult to control the final products obtained.

2.2.3b Nanocrystal Self-Assembly:

Self-assembly of nanocrystals involves the rearrangement of nanocrystals into single or multi-layered structures. The rearrangement is driven by entropy and, hence, favors the formation of the 2D structures.[143] It has been reported that the self-assembly process is also driven by dipole moments in the nanocrystals and due to the inherent hydrophobicity of the crystals.[144] The nanocrystals spontaneously reorganize their structures due to van der Waals interactions, electrostatic interactions, or hydrogen bonding.[145] The self-assembly process involves the fusing of the nanocrystals from their 3D structure into 2D oriented structures when external forces, such as pressure, are applied to the crystals (**Figure 4.4**).

Wang *et al*. synthesized PbS nanosheets by self-assembly of PbS crystals.[143] Stresses exceeding 11.6 GPa were applied to 3D crystal lattices of PbS, which prompted deviatoric stresses that produced 2D single-layered structure oriented in the direction of the stress being applied.

3 BIOLOGICAL APPLICATIONS

2D materials have been extensively researched for possible use in biosensors and bioimaging equipment. Biosensors are devices which convert biological responses or biomolecules of interest in the target into readable electronic or optical signals. Biosensors have been used for the detection of important biomolecules such as NADH,[146] DNA,[147] viruses,[148] and pathogenic bacteria.[149] 2D material-based sensors, especially graphene has shown superior sensitivity, mechanical properties and biocompatibility compared to its conventional counterparts like silicon. The higher sensitivity stems from the atomic thickness of 2D materials and large surface area-to-volume ratios, which places a majority of the atoms directly in contact with analytes.[150,151] These properties help in the creation of flexible, robust and commercially viable real time biosensing devices. The detection of DNA is an important application since it enables the detection of diseases before their onset by detecting specific sequences of damaged or mutated DNA. Detection and identification of DNA is also useful for applications in fields like forensics and the environment for the detection of genetically modified organisms, and pathogenic bacteria and viruses. Additionally, 2D material biosensors can be used to manufacture continuous glucose monitoring sensors with higher accuracy and longer lifetime. Bioimaging is the process in which real time biological processes are observed and imaged without invasive procedures using techniques like Magnetic Resonance Imaging (MRI), photoacoustic imaging (PA), or computed tomography (CT).[152]

2D materials have some unique properties such as high charge carrier density, high surface area, high interfacial area between the material and the electrode allow for high rates of electron transfer between the material and the sensing electrodes, making them suitable for use as the active sensing element in biosensor. These characteristics of 2D materials have inspired extensive research into the biological application of 2D materials in biosensors and bioimaging devices (summarized in **Table 1**). In this article, some of the recent advances of these biological applications are reviewed.

3.1 Graphene-based materials

Graphene and graphene oxide (GO) have shown potential to be used in a wide variety of biosensing and bioimaging devices. In contrast to graphene, GO has hydroxyl, epoxy, carbonyl, and carboxyl groups due to its highly oxidized nature, making it hydrophilic and

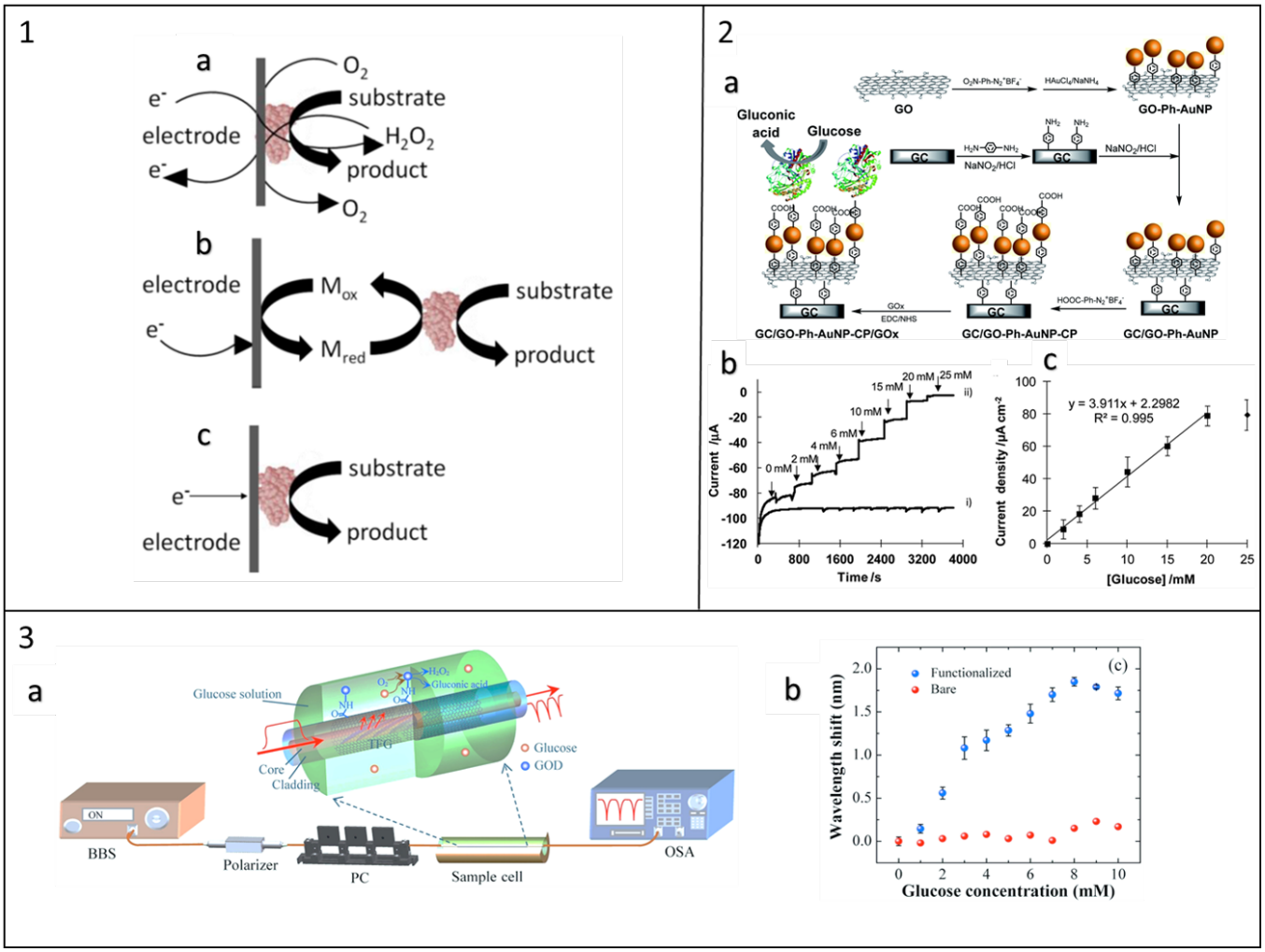

Figure 5 1) a-c) shows 1st generation to 3rd generation electrochemical biosensors. Reproduced from ref. [161], licenced under CC by 3.0 2) Schematic of glucose oxidase (labelled as GOx) immobilization on a graphene based biosensor developed by Qi et al. b-c)Graphs show the performance of the device w.r.t different glucose levels(i) is the control electrode with no immobilized glucose oxidase). Adapted from ref. [167] with permission from The Royal Society of Chemistry. 3- a) Schematic of a label-free glucose biosensor developed by Jiang et al. 3-b) The graph shows the measurement of glucose achieved by measuring shift of resonant wavelength of polarized light. Adapted with permissions from ref. [169]. Copyright 2018, Elsevier

readily dispersible in water. Therefore, GO is highly processable using traditional casting techniques like drop casting, spray coatings, etc.[153,154] The choice of processing method often yields unique GO morphologies like particles, sheets, fibers, and nanoribbons.[155–158] The GO can be reduced to graphene which retains some of this unique properties. For example, graphene fibers can be obtained by wet-spinning GO solutions followed by the chemical reduction of the fibers to graphene.[157] However, care must be taken to avoid a GO to graphene conversion, which is caused by a partial or incomplete electrochemical reduction on the surface.

Graphene and its derivatives are mainly produced via the Hummer's method.[159] In this method, graphite is oxidized with a mixture of sulfuric acid, sodium nitrate, and potassium permanganate to yield GO. Every atom in graphene is in direct contact with its environment and responds to electrostatic fluctuations caused by interactions with its environment, making it the perfect candidate for sensing applications.[160] A few 2D graphene-based devices are described below.

3.1.1 Enzymatic graphene biosensors:

The general development of electrochemical enzymatic biosensors is shown in Error! Reference source not found..**1**. In the first generation (Error! Reference source not found..**1.a)** of electrochemical biosensors, the electrode oxidizes and detects one of the naturally occurring chemical species in the enzymatic reaction pathway that occurs during detection of a molecule like glucose. Drawbacks of the system include the requirement of coenzymes, high potential for operation, and error caused by the dependence on electron acceptor concentration (such as dissolved molecular oxygen). The dependence on oxygen concentration and other drawbacks were addressed with the development of 2nd generation biosensors. 2nd generation biosensors (Error! Reference source not found..**1.b)** used synthetic mediators that act as electron shuttle molecules to transfer electrons to and from the substrate. In the 3rd generation the mediators are replaced by the principle of direct electron transfer between the enzyme and the electrode.[161–163] This electron transfer is detected and correlated to the concentration of

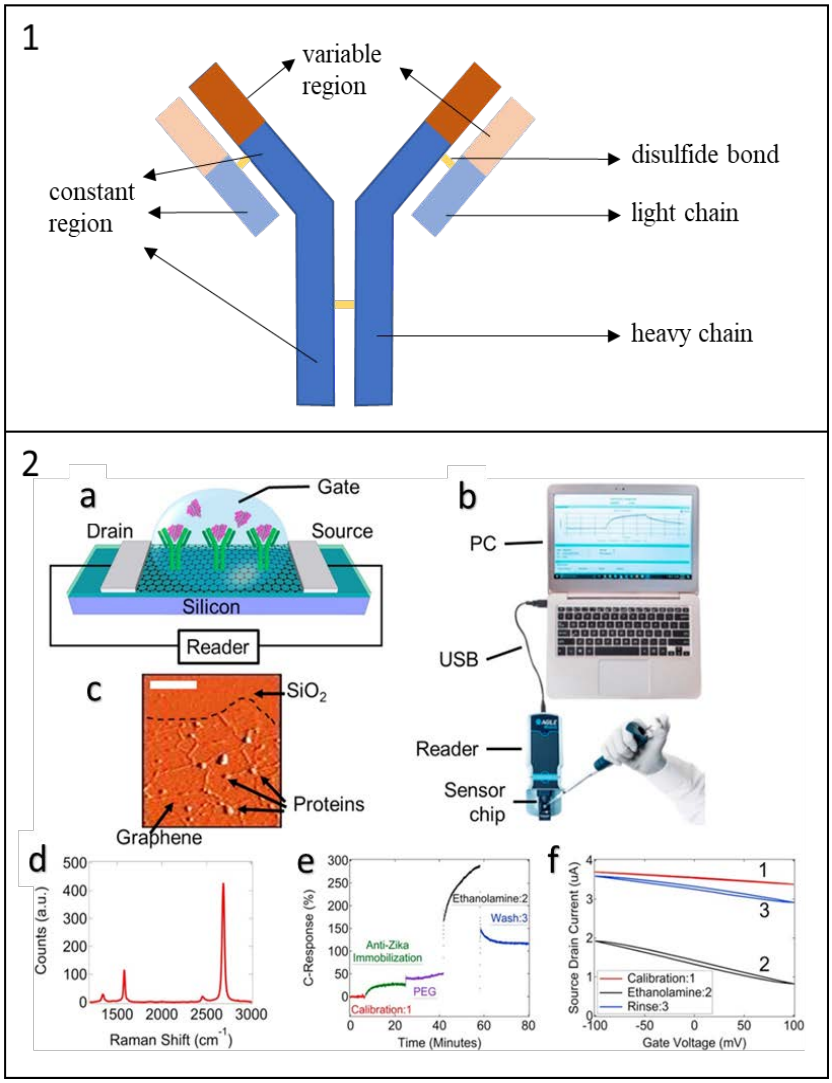

Figure 6 1) Schematic of an antibody 2- a) Diagram of the sensor element of a graphene biosensor chip with immobilized antibodies developed by Afsahi et al.(ref [148]) 2-b) Illustration of the entire sensor chip system, incorporating the sensor chip, reader electronics and digital control, and PC running control and data presentation software. 2-c) AFM image of the graphene after successful protein attachment, scale bar is 1 µm and Z height is 10 nm. 2-d) Raman spectrum after device fabrication demonstrating low D/G ratio, which indicates high quality graphene. 2-e) Percent change in capacitance during target immobilization and quenching on the graphene biosensor chip surface. 2-f) I-Vg curves at different immobilization steps. The dramatic steepening of the I-Vg slope indicates substantial change in the surface chemistry and increased sensitivity of the biosensor. Adapted from ref. 148, licensed under CC by 4.0

the molecule of interest. 3rd generation biosensors (Error! Reference source not found.**.1.c)** also do not require labels (an indirect species that probes the presence of the molecule of interest), are free from background interference, and have superior sensitivity[164] over the previous two generations.

The development of third-generation biosensors has expanded rapidly in recent years, especially in the current era of flexible, wearable electronics. The direct electron transfer mechanism between the redox center of an enzyme and the electrode is fundamental to the functioning of these devices. Pristine graphene has a high conductivity and large surface area, which makes it a functional material for electrochemical enzymatic sensing.[165,166] Graphene based materials have shown the intrinsic ability to immobilize some enzymes like glucose oxidase (GOD) and uricase via adsorption and covalent immobilization.[167–170] The ability to be tuned via functionalization and chemical modification makes it a unique platform for immobilization. This direct immobilization with the graphene based material acting as the electrode makes it an attractive platform for 3rd generation biosensors.[169–172] Enzyme-based graphene biosensors are typically electrochemical in nature.

Diabetes afflicts millions of people worldwide and has stimulated substantial research to develop accurate and rapid detecting sensors for blood glucose levels. GOD immobilized directly on electrodes are commonly used to design 3rd generation biosensors used to monitor blood glucose levels. Qi *et al*. decorated GO nanosheets with gold nanoparticles to make Glassy Carbon (GC)/GO-Ph-AuNP composites in order to immobilize GOD.[167] Glassy Carbon (GC) electrode surface was first modified with aryl diazonium salt to attach the GO-Ph-AuNP to the surface of the GC. Carboxylic acid groups were then added to this surface and GOD was then covalently bound via amide bonds to achieve the sensing interface as shown in Error! Reference source not found.**.2**. The sensor showed a

good linear response towards glucose with a sensitivity of 42 μA mM^{-1} cm^{-2} and with an enzyme turnover rate of 112 s^{-1}. A lab on fiber-optic glucose detection device (Error! Reference source not found.**.3.a**) was demonstrated by Jiang *et al*.[169] GOD-functionalized titled fiber grating (TFG) was made by the surface functionalization of the TFG; first, GO was deposited followed by the immobilization of GOD on the fiber surface. Monitoring the resonant wavelength shift in response to glucose concentration showed a linear response with the ability to sense concentrations in the range of 1-8 mM.

Marzo *et al*. recently used 3D printed graphene/poly(lactic acid) (PLA) electrodes to immobilize horseradish peroxidase (HRP) to create a 3rd generation electron transfer enzyme-based sensor for detecting hydrogen peroxide.[173] In addition, AuNPs were used to confirm the direct electron transfer between the HRP and 3D-printed graphene-PLA electrode. The AuNPs slightly enhanced the biosensor performance from a Limit of Detection (LOD) of 11.1 μM to 9.1 μM. The analytical range for the measurement was 25-100 μM concentrations of hydrogen peroxide. This work further highlights the ability of graphene to immobilize enzymes and act as a biosensor.

3.1.2 Antibody graphene biosensors:

In these types of devices, the analytical detection platform measures specific conjugation reactions between antigens and antibodies. Antibodies are immunoglobulin monomer globular plasma proteins consisting of four polypeptide chains with a characteristic "Y" shape. Immunoglobulin G (igG) is the most commonly used class of antibody for biosensing. It consists of two heavy protein chains and two light protein chains that are connected via disulfide bonds as shown in **Figure .1**. The arms of the antibody consist of a constant and variable domain. The variable domain imparts selectivity of the antibody to a specific antigen.[174]

Afsahi *et al*. demonstrated a cost-effective and portable graphene-enabled biosensor (**Figure .2**) to detect the Zika virus. [148] Anti-Zika NS1 antibodies were immobilized on pristine graphene, and the remainder of the surface is then blocked and passivated to reduce nonspecific interactions. To detect the Zika virus, the device measures shifts in the channel current and gate capacitance of the graphene caused by interactions with specific biological targets; these device are commonly referred to as biosensing field effect transistor (FET) or field effect biosensors (FEB).[148]

Mao *et al*. developed a FET selective towards specific proteins. Vertically oriented graphene sheets are grown directly on a sensor electrode using plasma-enhanced CVD and labelled with AuNP-antibody conjugates.[175] The binding of the probe to target proteins induces significant changes to the electrical conductivity of the FET sensor. The device shows high sensitivity down to 13 pM of the analyte protein, IgG. It is important to note that both devices described above make use of the fact that graphene is highly sensitive to electrical perturbations, due to its 2D nature and high carrier mobility. Therefore, any change that occurs from the protein binding induces a measurable change in the electrical conductivity.[148,175]

3.1.3 Graphene DNA biofunctionalization

The planar, conjugated nature of graphene enables strong π-π stacking interactions with deoxyribonucleic acid (DNA) nucleobases. For example, single stranded DNA (ssDNA) has been reported to bind to graphene with high affinity through π-π stacking interactions.[160,165,176,177]

Hao et el. reported real time monitoring of insulin using a Graphene Field-Effect Transistor (GFET) aptameric nanosensor.[178] This label-free method uses an aptameric receptor, IGA3, which specifically binds to insulin. Insulin levels as low as 35 pM can be detected with a response time below 260 s. IGA3 is functionalized onto the graphene surface through a Schiff-base reaction using a 1-pyrenebutanoic acid succinimidyl ester (PASE) linker immobilized in graphene. The aptamer binds to insulin promoting formation of parallel and anti-parallel G-quadruplexes which brings the negatively charged insulin and DNA strands closer to the vicinity of the graphene surface. The proximity changes carrier density in the graphene bulk yielding detectable signals.

In another example, a GFET molecule-specific probe was developed by Dontschuk *et al*.[147] The device was shown to have distinct conductance signatures upon adsorption of four difference DNA nucleobases which can pave the way towards next-generation DNA sequencing technologies. Xu *et al*. utilized a multi-channel GFET DNA sensor array for real-time determination of binding kinetics of DNA hybridization. The detection limit of the device was 10 pM for DNA and it was able to distinguish single-base mutations quantitatively in real time.[179] The adsorption of DNA onto the GFET devices, induced dipoles on the four different DNA nucleobases, which were correlated to distinct conductance signatures detected by the GFET.

3.1. Graphene for bioimaging

Bioimaging is an integral part of both research and clinical practice. This allows the observation and study of biological processes ranging from cells to small animals.[152] This can also be used as a powerful tool for early stage disease detection and monitoring of treatment response. Graphene quantum dots (GQDs) and nanographene exhibit a low cytotoxicity, strong photoluminescence, magnetic resonance signatures, tunable fluorescence, etc., and are attractive candidates that can used in next generation bioimaging devices.[180,181]

GQDs were discovered by Ponomarenko *et al*. in 2008[182] and are superior in comparison to traditional semiconductor quantum dots because of their lower toxicity, higher biocompatibility, improved chemical inertness, and enhanced solubility.[183] While GQDs are not 2D materials, they do exhibit some of the quantum phenomena that make 2D materials interesting and useful in biological applications. GQDs can be doped with nitrogen to tailor the optical and electrical properties of the quantum dots, which was first realized by Li *et al*. and resulted in blue

luminescence.[184] The key factor affecting the photoluminescence intensity is the n-π* transition between the nitrogen in the aromatic ring and the conjugate structure of graphene. Nitrogen doping is the most widely used method to improve photoluminescence quantum yield in GQDs.[185,186] Other dopants, such as boron, sulfur, phosphorus, fluorine, etc., can also be used, but additional research is needed to fully understand how the amount and type of dopant affects the material properties. Though these offer unique optical and electrical properties, the quantum yield from these dopants remain relatively low due to non-radiative recombination processes enabled by the dopant/defect engineering process.[187–189]

GQDs from Mangifera indica (mango) leaves were reported to be produced by a simple one-pot microwave assisted green synthesis route by Kumawat *et al*.[190] The GQDs were 2-8 nm in diameter and exhibited bright red luminescence. A cellular uptake study using flow cytometry showed 100% of the cells were internalized compared to control cells. Furthermore, a biocompatibility study using the MTT assay showed that more than 95% of mouse fibroblast L929 cells were viable after 24 h at a concentration range of 0.1 - 5 mg mL^{-1}. An inverse relationship between fluorescence intensity and temperature allowed the GQDs to be used for temperature sensing applications. In another study, a hydrothermal route to synthesize the N-doped GQDs with multiple color emissions was demonstrated by Qu *et al*.[191] Depending on the reaction solvent nature (protic, aprotic, solvent free) the emission of the N-doped GQDs shifted from blue to green to yellow, respectively.

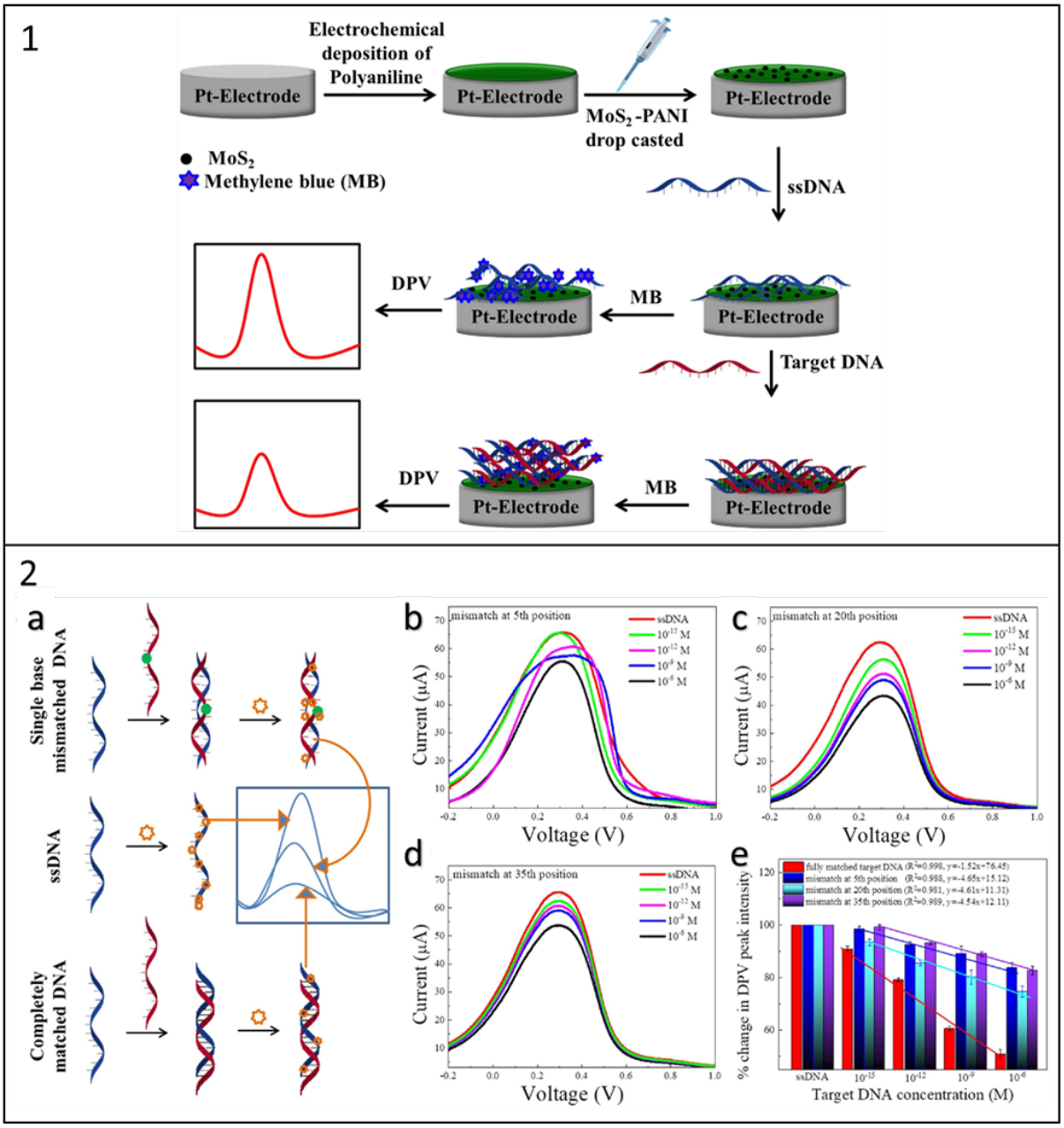

Figure 7. 1) Schematic representation of the fabrication steps of an electrochemical sensor for DNA hybridization and DPV metric detection. 2 (a) Schematic illustration of the DPV signal of Pt||MoS_2-polyaniline-ssDNA electrode with completely matched and single base mismatched DNA, DPV of Pt||MoS_2-polyaniline-ssDNA electrode with different concentration of single mismatched DNA at position of (b) 5th, (c) 20th and (d) 35th, (e) comparative bar diagram of percentage change of DPV signals with completely matched and three positional single mismatched target DNA in a concentration range of 10^{-15} to 10^{-6} M. Adapted with permissions from ref. [194]. Copyright 2018, Elsevier.

Different solvents change the effective π-conjugation length and the dopant concentration in the GQD framework. The polar aprotic solvent (*N*,*N*-dimethylformamide) increased the π-conjugation length and dopant content whereas the polar protic solvent (H_2O) decreases both. Therefore, the emission band of N-doped GQDs can be tuned based on the solvent properties. After incubation with the N-doped GQDs (3 mg mL^{-1}) at 37 ˚C for 1 h, human lung epithelial (A549) cells under living conditions were imaged using a confocal fluorescence microscope to demonstrate imaging at different excitation wavelengths (i.e., 405, 388 and 555 nm).[191]

Chen *et al*. reported the development of reduced graphene oxide (rGO) based hybrid nanostructures with covalently attached Fe_2O_3@Au core@shell nanoparticles (rGO–Fe_2O_3@Au NPs).[192] These nanostructures were examined as potential magnetic resonance imaging (MRI) theranostic contrast agents, which can be used for imaging in combination with drug delivery. Specifically, the nanostructure composition enables MRI, and the structure allows for the transport and delivery of a chemotherapy drug, such as doxorubicin (DOX); moreover, when the nanostructure is exposed to the magnetic field it releases the drug, enabling imaging and targeted drug delivery. An MTT assay of cytotoxicity toward HeLa cells showed that the cell viability when exposed to rGO–Fe_2O_3@Au NPs remained above 90% at concentrations as high as 50 μg mL^{-1}, confirming low cytotoxicity. The cell viability decreased with the increase in DOX concentration brought about by magnetic field-assisted release of DOX. The all-in-one nanoplatform paves a straightforward route to develop multifunctional theranostic agents for magnetic-guided synergistic chemo-photothermal therapy of cancer.[192]

3.2 Transition Metal Dichalcogenides:

As described above, many biosensors employ FETs due to their advantages such as fast electrical detection, low power consumption, and the possibility for integrating both the sensing and the measuring parts onto a single chip.[31] FET biosensors made using MoS_2 as the semiconducting material are widely used in biosensing equipment to detect DNA, proteins, and other biomolecules.

3.2.1 DNA biosensors:

Lee *et al*. reported the fabrication of a bioelectronic–FET (bio-FET) using MoS_2 as the active sensing channel fabricated onto a p-type Si wafer with a 300 nm SiO_2 layer.[193] ssDNA molecules were immobilized onto the MoS_2 layer for the detection of DNA molecules through DNA hybridization. DNA hybridization involves the binding of the target DNA with the immobilized ssDNA, which causes the release of electrons that are then transferred to the active layer. The direct immobilization of the target DNA and its subsequent hybridization with the ssDNA strands on the active layer surface allow for the detection of DNA molecules at concentrations as low as 10^{-2} pM. The range of detection shifts by a factor of 10^6 if the DNA being hybridized with the probe DNA is changed from complementary DNA to non-complementary DNA with a single base-pair mismatch. This MoS_2 based bio-FET can be used in areas such as disease diagnosis, food safety, and forensics.

Dutta *et al*. reported a biosensor with MoS_2 incorporated into polyaniline for sensing DNA molecules.[194] MoS_2 incorporated into polyaniline was chosen as the active channel onto which ssDNA was immobilized, which was coated onto platinum electrodes (**Figure 7)**. A methylene blue dye was used as a redox indicator for the signify DNA hybridization since it specifically binds to both ssDNA and double stranded DNA (dsDNA). The sensor could measure DNA in concentrations ranging from 10 pM to 10^3 pM. The sensor was stable in a pH ranging from 4 to 9, and, in addition, to being able to detect DNA, it could also detect any DNA mismatches.

A photoelectrochemical biosensor based on protonated graphitic carbon nitride (P-g-C_3N_4), WS_2, Au-NPs, and ITO with MnO_2 nanoflowers as signal quenchers (**Figure 8**) was developed by Yin and coworkers.[195] The Au-NP/(P-g-C_3N_4)/WS_2/ITO was developed to detect DNA formylation by detecting 5-formylcytosine (5fC), a biomarker for oxidative damage to DNA. It is an important intermediate oxidation product that plays an important role in human diseases and gene regulation, which makes it an important biomolecule to be monitored. The problem with 5fC is that it is present in very low concentration in mammalian cells, hence it is important for a biosensor with a high sensitivity to 5fC to be discovered. The P-g-C_3N_4/WS_2 nanocomposite sheets were prepared using the electrostatic self-assembly methods and the biosensor was prepared by drop-casting the P-g-C_3N_4/WS_2 nanocomposite onto the bare ITO electrodes after which the probe ssDNA solution was immobilized on the active surface. The detection of 5fC in the test DNA solution is achieved by detecting the photocurrent between the biosensor, a platinum counter electrode, and a calomel reference electrode. It was reported that the linear detection range was 10 pM to 2×10^5 pM with the detection limit being 3.8 pM. This method has the advantage of having high specificity, low detection limits, use of inexpensive instruments, and ease of operation.

3.2.2 Biosensors for other biomolecules:

Detecting the concentration levels of biomolecules is important for monitoring various metabolic processes. For example, monitoring insulin levels and blood glucose concentrations is important for individuals suffering from diabetes mellitus, whereas monitoring the levels of NADH and its oxidized form, NAD^+, can provide insight into energy metabolism. Selvarani *et al*. developed a $MoSe_2$/hydrogen exfoliated graphene (HEG) hybrid electrode for the detection of NADH.[146] The $MoSe_2$ nanosheets were exfoliated in the liquid phase and then sonically exfoliated onto the HEG sheets. The electrode was prepared by drop-casting the $MoSe_2$/HEG nanosheet solution onto a highly polished GC electrode. The detection of NADH is done by measuring the redox current generated at the electrode-electrolyte interface by the oxidation of NADH to NAD^+. The sensor showed sensitivity as high as 0.0814 μA $μM^{-1}$ ranging from 1 μM to 280 μM and had a good selectivity when compared to the standard

enzyme based NADH assays. The high performance was attributed to the homogeneous dispersion of $MoSe_2$ over the HEG sheets, which acts as an electron transfer channel while retaining its electrochemical activity and preventing restacking.

Khataee *et al.* reported a WS_2 nanosheet/Ag-NP nanocomposite with peroxidase mimicking behaviour that was used to detect blood glucose levels.[196] The enzyme, GOD, oxidizes glucose to gluconic acid and produces H_2O_2 as a byproduct. The concentration of H_2O_2 is directly related to the concentration of glucose in the sample, which can be used to measure glucose levels. The sonically exfoliated WS_2 nanosheets were loaded with Ag-NPs, which were then loaded onto a GC electrode. Colorimetric, electrochemical, and fluorescence experiments were carried out to determine the peroxidase mimicking capability of the prepared nanocomposite out of which, the fluorescence system was chosen for the detection of glucose and H_2O_2 due to its higher sensitivity. The system showed a linear detector response for H_2O_2 over the range of 0.01-2 µM with a limit of detection being 0.26 nM. Similarly, it exhibited a linear detector response for glucose in the range of 0.05-400 µM with a detection limit of 21 nM.

Glycated haemoglobin (HbA1c) is an important biomarker which can be used to detect type I and type II diabetes. HbA1c is a better biomarker than plasma glucose for monitoring the glycaemic levels and for the diagnosis of type I and type II diabetes since the glucose levels in plasma fluctuate widely, whereas glycated haemoglobin has a more consistent concentration over longer periods of time. Yang *et al.* reported a biosensor using WS_2 nanosheets which were functionalized by boronic acid-modified poly(vinyl alcohol).[197] HbA1c quenches the fluorescence of B-PVA/WS_2 nanosheets which can be used as a detecting mechanism wherein the fluorescence quenching is linearly dependent on the concentration of glucose. The synthesized B-PVA/WS_2 nanosheets were able to detect HbA1c at concentrations as low as 3.3×10^{-4} pM.

A surface plasmon resonance immunosensor based on MoS_2 functionalized fiber optic was developed by Kaushik *et al.*[149] The fiber optic was first etched, and then coated with a gold layer onto which the MoS_2 nanosheets, which were prepared by sonication-assisted liquid exfoliation, were dip-coated onto the fiber optic cable. *E. coli* monoclonal antibodies were immobilized onto the surface of the MoS_2/Au/optical fiber cable for the detection of *E. coli.* The detection of *E. coli* was based on the shift in the resonant frequency when the antibody-antigen complex is formed. The sensor has an *E. coli* detection range of 1000-8000 CFU mL^{-1} and the limit of detection was reported as 94 CFU mL^{-1}. Although this specific biosensor detects bacteria over a range of concentrations, further

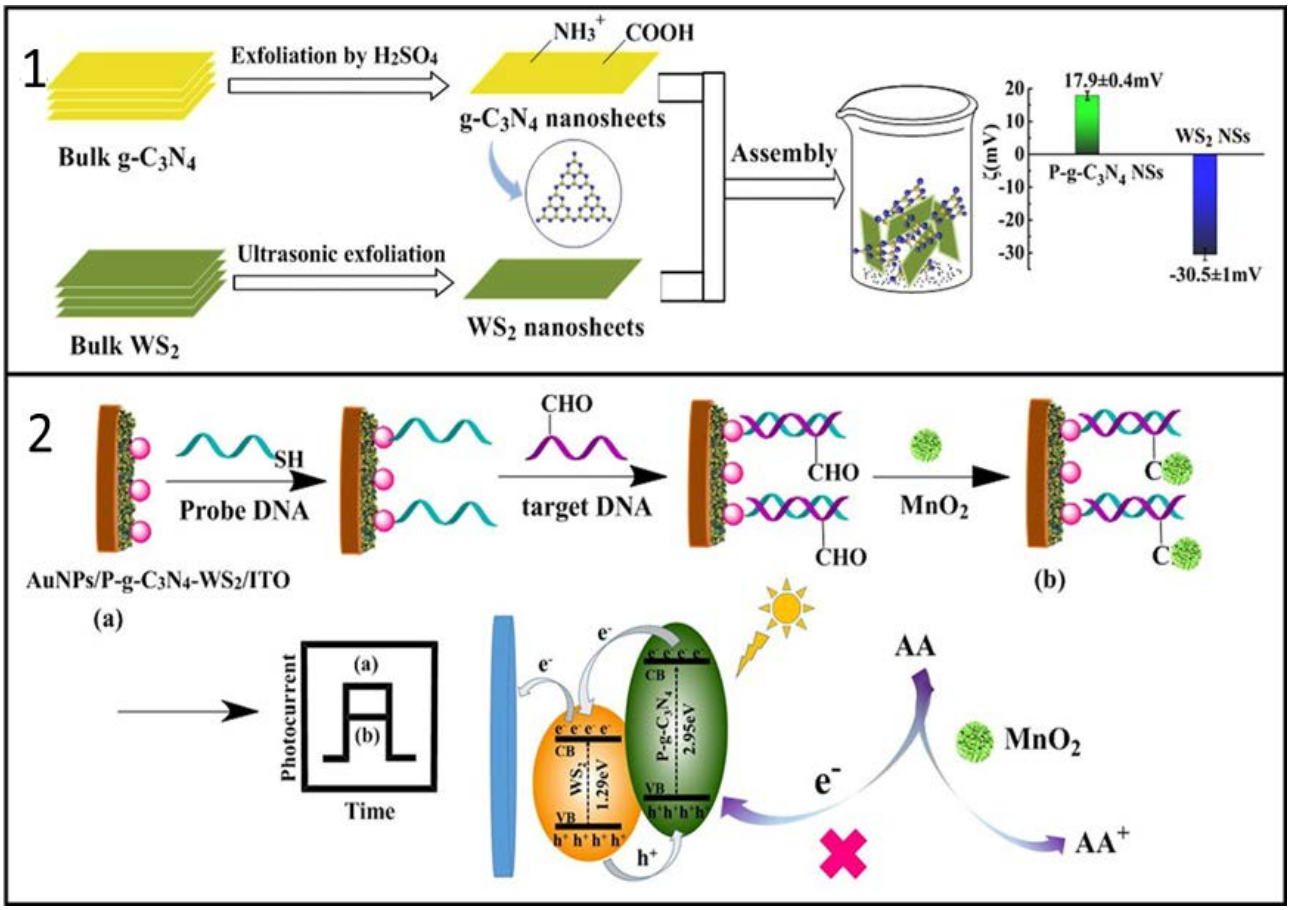

Figure 8 1) Preparation principle of P-g-C3N4-WS2 composite. 2) construction process of PEC biosensor. Adapted with permission from ref. [195]. Copyright 2020, Elsevier

research must be done to decrease the cost of manufacturing for a commercially viable biosensor.

3.3 Transition Metal Oxides:

Transition Metal Oxides (TMOs), although not as extensively studied for biosensor applications as TMDs and other 2D materials, have also been used in the fabrication of biosensors.

Ran *et al.* synthesized a DNA-based biosensor with DNA immobilized onto MnO_2 sheets for accurate differentiation of cell types for the detection of diseases.[198] Non-specific DNA strands with guanine-rich regions were used as the DNA probes. N-methyl mesoporphyrin IX (NMM), a ligand which binds with G-quadruplex present in guanine-rich DNA was used as the fluorescence causing agent. The NMM bonded DNA probes were immobilized onto the MnO_2 through physisorption, where the MnO_2 nanosheets act as fluorescence quenchers. This biosensor ensemble would then be absorbed into the cell through endocytosis, where the NMM-binding DNA probe would disassemble from the nanosheets inside the cell, leading to a recovery in fluorescence. The relative changes in the fluorescence intensity depended upon the interaction between the cell and the DNA strands which were different to each type of cells which could be used in the identification of the type of cells. A total of 40 samples were tested, each with 5 different types of DNA probes. This biosensor was able to differentiate between 8 different cell types in the tested samples and it also identified cells types from unknown samples with 95% accuracy.

A colorimetric biosensor based on Human Serum Albumin (HSA) templated-MnO_2 nanosheets for the detection of glutathione (GSH) was developed by Ge *et al*.[199] The HSA templated MnO_2 nanosheets are able to catalyse oxidation of 3,3',5,5'-tetramethylbenzidine (TMB), a colourless compound to a blue oxTMB compound with an absorption peak at 652 nm, suggesting oxidase-like behaviour. In the presence of GSH, the oxidation of TMB to oxTMB does not occur since GSH reduces MnO_2 to Mn^{2+}, reducing its catalytic behaviour. This inhibition of the oxidation of TMB to oxTMB in the presence of GSH is concentration-dependant, implying that this can be utilized as a colorimetric detection method for GSH. The biosensor had a range of detection from 10^4 to 5 x 10^6 pM with a limit of detection at 5.6 x 10^3 pM.

An In_2O_3 thin film transistor (TFT) based biosensor was synthesized for the detection of biotin, also known as vitamin H by Yang *et al*.[200] The detection of vitamin H is clinically important for tumour-targeted cancer therapeutics. The In_2O_3 thin layer was synthesized by metal organic chemical vapour deposition (MOCVD). Streptavidin was used as a receptor for biotin, which when introduced onto the aldehyde-functionalized surface of In_2O_3, causes a negative change in the surface potential of the TFT. When biotin binds with Streptavidin, there is an increase in the flow of current through the TFT which is used as the detecting mechanism. The biosensor had a limit of detection at 5 x 10^4 pg mL^{-1}.

3.4 Other analogues of Graphene:

Graphene analogues have been employed in the fabrication of biosensors owing to their properties discussed earlier in the article such as high carrier mobility, tuneable band gaps, very high surface areas and compatibility with biomolecules.

A novel graphene quantum dots (GQD)/h-BN nanosheet molecularly imprinted polymer biosensor for the detection of serotonin was synthesized by Yola *et al*.[201] Serotonin is an important hormone in the human body. Low or high amounts of serotonin in the body can lead to seizures and muscle rigidity and hence must be monitored. For the biosensor, sonication-assisted liquid exfoliated h-BN nanosheets were synthesized and a GQD/h-BN nanocomposite was synthesized. The nanocomposite was drop casted onto a glassy carbon electrode (GCE) onto which a serotonin-polymer solution was added. The serotonin was washed off with 1M NaCl solution to create a serotonin molecular imprinted polymer (MIP)/GQD/h-BN biosensor which was used for the detection of serotonin. The biosensor had a linear detection range from 1 pM to 10^4 pM with a detection limit of 0.2 pM.

Despite environmental instability issues of black phosphorus (BPs) layers, a BP-based fiber optic biosensor for the detection of neuron-specific enolase (NSE) was explored by Zhou *et al*.[202] NSE is a highly specific biomarker used to detect specific tumours like lung cancer, medullary cancer etc. The BP nanosheets were synthesized by sonication-assisted liquid exfoliation, which were then deposited onto a fiber optic with a tilted fiber grating using an in-site layer-by-layer deposition technique in which the BP nanosheets physically adsorbed onto the fiber optic. The BP nanosheets were biofunctionalized by poly-L-Lysine and anti-NSE biomarkers were covalently immobilized onto poly-L-Lysine. The binding of the NSE enzymes onto the anti-NSE markers on the fiber optic increases the concentration of the NSE enzymes on the surface, thereby changing the local refractive index, causing a wavelength shift through the fiber optic. The Limit of Detection for this biosensor was 1 pg mL^{-1} and the sensitivity for the NSE biomarkers was also 100-fold higher than gold-nanoparticles- or graphene oxide-based biosensors.

3.5 2D nanopore DNA sensors

Solid state silicon based nanopores devices can sequence DNA molecules by threading the molecules through a pore under an applied potential and monitoring the ionic current passing through the pore.[203–206] The single-atom thickness of graphene and other 2D materials makes them comparable in dimensions to the spacing between two neighbouring nucleotides along single strand DNA (ssDNA). This promises single-base resolution in the ionic current measurements .[207–210]

Traversi *et al.* showed the integration of a solid-state Silicon Nitride (SiN_x) nanopore with a graphene nanoribbon transistor for DNA translocation.[207] The resulting device structure is

Table 1 Performance of different 2D biosensors

Author	Material	Target Biomolecules/ Microorganism	Range and Limit of Detection (ROD/LOD), Sensitivity	Additional Comments
Graphene-based Biosensors				
Qi *et al.*[167]	Graphene Oxide (GO) with Au Nanoparticles (NP)	Glucose	ROD: $3 \times 10^8 – 2 \times 10^{10}$ pM LOD: 3×10^8 pM Sensitivity: 42 μA $mM^{-1}cm^{-2}$	-
Jiang *et al.*[169]	GO deposited on optical fiber grating	Glucose	$10^6 – 8 \times 10^6$ pM Sensitivity: 0.24 nm mM^{-1}	-
Luo *et al.*[211]	Graphene- Cu NP	Glucose	ROD: $5 \times 10^8 – 4 \times 10^9$ pM LOD: 5×10^8 pM Sensitivity: 1234 μA mM^{-1} cm^{-2}	
Zhang *et al.*[212]	Glassy carbon electrode with N-doped rGO and $Ni(OH)_2$	Glucose	ROD: $5 \times 10^5 – 1.15 \times 10^7$ pM LOD: 1.2×10^5 pM Sensitivity: 3760 μA mM^{-1} cm^{-2}	
Vilian *et al.*[213]	rGO/ZrO_2 NP	Glucose	ROD: 29×10^7 -14×10^9 mM LOD: 0.13 mM Sensitivity: 11.65 μA mM^{-1} cm^{-2}	
Halder *et al.*[214]	rGO/polyethyleneimine composite	Glucose	ROD: 0.1 – 15.5 mM LOD: 5 μM Sensitivity: 3.45 mA M^{-1} cm^{-2}	
		Cholesterol	ROD: 2.5 – 25 μM LOD: 0.5 μM Sensitivity: 380 mA M^{-1} cm^{-2}	
Marzo *et al.*[173]	3D printed Graphene - AuNP - Poly lactic acid	Hydrogen Peroxide	LOD: 1.11×10^7 pM (without AuNP); 0.91×10^7 pM ROD: $2.5 \times 10^7 – 10^8$ pM	Addition of AuNP increases the limit of detection.
Afsahi *et al.*[148]	Graphene on silicon chip	Zika Virus	LOD: 450 pM	-
Mao *et al.*[175]	Graphene with AuNP-antibody conjugate	Proteins	Sensitivity: 2 ng mL^{-1}	-
Hao *et al.*[178]	Graphene based Field Effect Transistor (FET)	Insulin	LOD: 3.5×10^7 pM	The biosensor had a response time below 260 seconds
Dontschuk *et al.*[147]	Graphene based FET	DNA nucleobases	Sensitivity: 0.1 monolayer for guanine	-
Xu *et al.*[179]	Multi-channel Graphene based FET	DNA	LOD: 10 pM	Biosensor able to distinguish between different single base mutations quantitatively in real-time
Transition Metal Dichalcogenides (TMDs)-based biosensors				
Khataee *et al*.[196]	WS_2 – Ag NP	Glucose	ROD: $5 \times 10^4 – 4 \times 10^8$ pM LOD: 2.1×10^4 pM	-
Geng *et al.* [215]	Ni-MoS_2/rGO composite	Glucose	ROD: 5×10^6 - 8.2×10^9 pM LOD: 2.7×10^6 pM Sensitivity 256.1 μA cm^{-2} mM^{-1}	Rapid response time of 2 seconds
Wu *et al.*[216]	Ultrathin MoS_2 nanosheet photoanode	Glucose	ROD: 8×10^3 -5×10^6 pM LOD: 600 pM	
Lee *et al*.[193]	MoS_2 on p-type Si layer	DNA	ROD: dynamic range of 10^6 LOD: 0.01 pM Sensitivity: 17 mV/dec	-
Dutta *et al*.[194]	MoS_2-Poly aniline	DNA	ROD: $10^{-3} – 10^6$ pM LOD: 10^{-3} pM Sensitivity: 0.0814 μA $\mu M^{-1}cm^{-2}$	-
Yin *et al*.[195]	Protonated- graphitic carbon nitride (g-C3N4)-WS_2 with ITO and MoS2 as signal quenchers	5-formyl cytosine (5fC)	ROD: $10 – 2 \times 10^5$ pM LOD: 3.8 pM	-
Selvarani *et al*.[146]	$MoSe_2$ – Hydrogen exfoliated graphene	NADH	ROD: $10^6 – 2.8 \times 10^8$ pM LOD: 10^6 pM	-

Yang *et al*.[197]	WS_2- boronic acid modified poly vinyl alcohol	Glycated Haemoglobin (HbA1C)	LOD: 3.8×10^4 pM	- -
Kaushik *et al*.[149]	MoS_2 nanosheets on a gold-layered fiber optic	E. Coli	LOD: 94 CFU mL^{-1} Sensitivity: 2.9 nm/1000 CFU mL^{-1}	
Transition Metal Oxides (TMOs)-based biosensors				
Ran *et al*.[198]	MnO_2	DNA (for the detection of cell types for disease detection)	N/A	-
Ge *et al*.[199]	Human Serum Albumin templated – MnO_2	Glutathione	ROD: 10^4 - 5×10^6 pM LOD: 5.6×10^3 pM	-
Yang *et al*.[200]	In_2O_3	Vitamin - H	LOD: 50 ng mL^{-1} Sensitivity: 150 nA dec^{-1}	-
Analogues of Graphene				
Wu *et al*.[217]	Platinum NP modified polyaniline-functionalized Boron nitride nanotubes	Glucose	ROD: 10^7 - 5.5×10^9 pM LOD: 1.8×10^5 µM Sensitivity: 19.02 mA $\mu M^{-1} cm^{-2}$	
Ranganethan *et al.*[218]	h-BN -Cu- MOF composite	Glucose	ROD: $10^7 – 900 \times 10^9$ pM LOD: 5.5×10^6 pM Sensitivity: 18.1 µA μM^{-1} cm^{-2}	
Yola *et al*.[201]	GQD/hexagonal Boron Nitride (h-BN)	Serotonin	ROD: $1 – 10^4$ pM LOD: 0.2 pM	-
Zhou *et al*.[202]	Black Phosphorus	Neuron-specific Enolase	LOD: 1 pg/mL	Enhanced sensitivity of the biosensor is 100-fold higher than GO- and AuNP- based sensors

a graphene nanoribbon defined on a SiN_x membrane with a nanopore located at the center. This was used to detect translocation of circular plasmid pNEB DNA (2,713-bp-long derivative of pUC19 plasmid) in 10mM – 1 M KCL buffer. The ionic current and the electrical current flowing through the GNR during DNA translocation was simultaneously recorded. 923 events were observed in the graphene channel (41% correlated) and 532 events in the ionic channel (71% correlated) with amplitudes of 5nA and 1 nA, respectively.

Graphene has strong hydrophobic interactions with DNA nucleotides, causing the DNA to eventually stock to the graphene nanopores.[210,219,220] Thus further surface treatments to reduce these interactions are required for the functioning of graphene nanopores. MoS_2 nanopore membranes on the other hand do not exhibit these interactions and require no additional surface treatments. [208] Liu *et al.* presented a 2D MoS_2 nanopore membrane with a signal-to-noise ration performance improvement of over 10 times in comparison with thicker conventional SiN_x nanopores.[20] The device also exhibited a signal amplitude that is five times higher than SiN_x nanopores. The MoS_2 is suspended on a pre-etched-square shaped opening on 20 nm thick supporting SiN_x membranes. This enjures that the DNA can translocate through the sub-nanometer thick MoS_2 instead of the 20 nm thick SiN_x. The device showed good stability at high ionic strengths with a low failure rate and was successful in threading double stranded DNA (dsDNA) of different lengths and conformations. A study by the same group later explored the effect of geometry in 2D nanopores.[20] Geometry dependant ion scattering was observed when comparing triangular h-BN nanopore with circular MoS_2. The DNA induced conductance drop in MoS_2 nanopores were found to be superior to that in h-BN nanopores, due to higher ion flux through the former.

4 TOXICOLOGICAL EFFECTS OF 2D MATERIALS

The diverse and unique physicochemical properties of 2D materials allow for a wide range of biological and biomedical applications. Most research on these exciting materials has been focused on exploring the synthesis, properties, and potential applications. Despite the potential of 2D materials in biological and environmental applications, the inherent toxicity and biocompatibility needs to be investigated before further exploration and subsequent development of these materials into impactful products.

Figure 9 shows a Scopus search on the number of articles published on 2D materials and on toxicity of 2D materials. It is evident that, even with a steady increase in the number of articles being published on both 2D materials and 2D material toxicity, there is a large gap between the number of studies done on 2D materials and studies on their toxicological effects. More research must be done to elucidate the toxicological effects of 2D materials to fill the huge gap in knowledge left by this trend. Proactive studies into the biological and environmental interactions of 2D materials will direct appropriate material synthesis and systems, as well as identify potential risks that can be mitigated prior to implementation. There

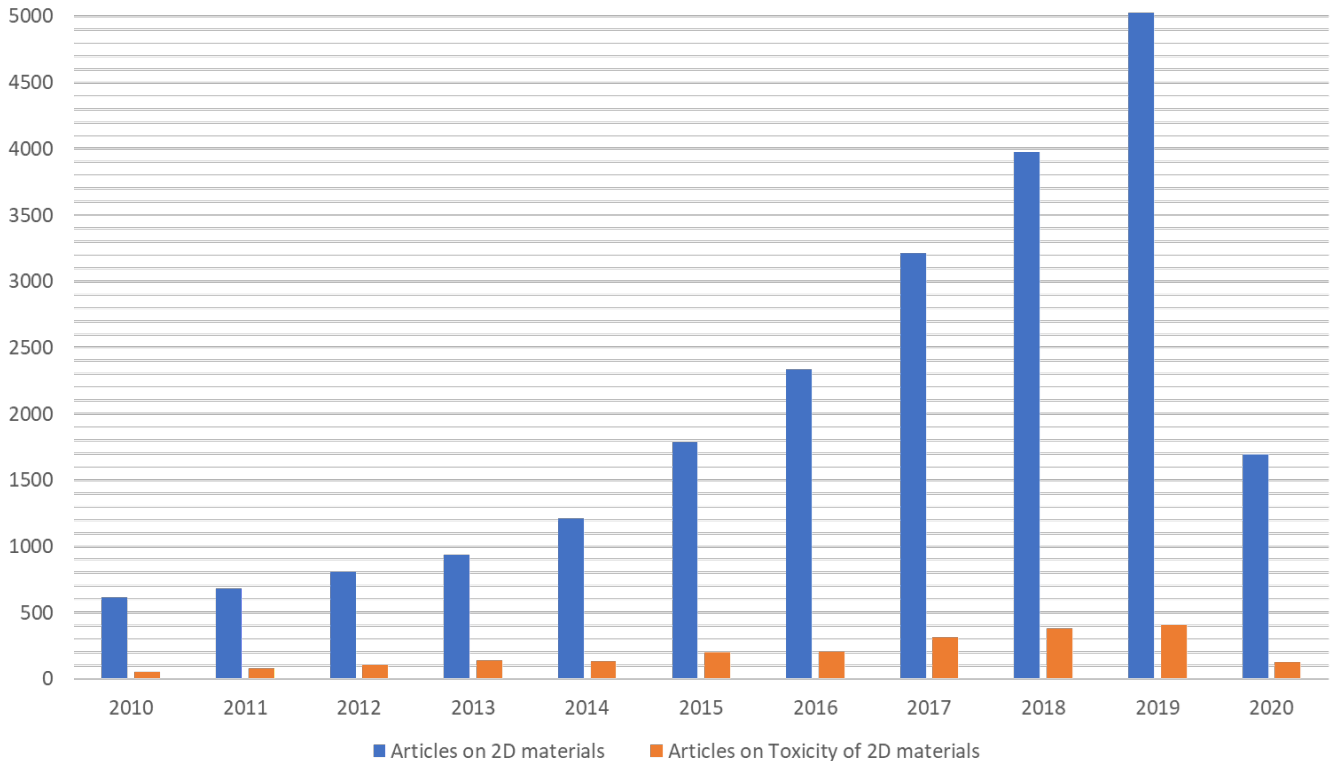

Figure 9 Scopus search of articles published on 2D materials research and toxicology of 2D materials. The keywords "2D material", "toxic", “toxicity”, "biocompatible", "biocompatibility" and "toxicology" were used as keywords for the search. The graph is based on scopus results obtained on April 8th 2020.

are limited recent articles summarizing the toxicity of 2D materials, specifically graphene, hexagonal boron nitride, MoS_2, and several other TMDs.[221–224] Some of them are discussed below with a focus on graphene and TMD toxicology studies.

For the case of graphene, there have been multiple conflicting reports about the biocompatibility and toxicity of graphene-based materials.[225] It is generally agreed that depending on the type of graphene material, lateral dimension, concentration, functionalization, dosage, and cell line, the cytotoxicity effect of graphene-based materials can be drastically different.[222–224,226–228] A study by Chong *et al*. found no obvious *in vitro* and *in vivo* toxicity of GQDs even with multi-dosing.[229] The low *in vitro* cytotoxicity was attributed to the ultra-small size of GQDs and high oxygen content. *In vivo* biodistribution experiments of the GQDs revealed no bio-accumulation in the main organs of mice and exhibited fast clearance of the particles through the kidney. However, in another study GQDs were shown to cause DNA damage in NIH-3T3 cells, without any obvious toxicity being observed at a cellular level. The DNA damage was indicated by an increased expression of several proteins (e.g., p53, Rad 51, and OPGG1) related to DNA damage when compared with controls.[230] Pelin *et al*. studied the cytotoxic effects of graphene and graphene oxide on skin keratinocytes (HaCaT) to monitor skin toxicity.[231] Four materials, including two research grade graphene-based materials: ball milled few layer graphene (FLG), and graphene oxide 1 (GO1, prepared by the common Hummer's method), and two commercial GOs: prepared using two different starting materials (carbon nanofibers, GO2, and graphite, GO3) were used in the study. FLG, GO1, GO2, and GO3 had average lateral dimensions of 552, 622, 845, and 979 nm, respectively. A water soluble tetrazolium salt (WST)-8 assay on HaCaT showed that the GOs and especially the FLG caused very weak cytotoxicity on skin keratinocytes. While no significant reduction in mitochondrial activity was observed after 24 h, mitochondrial activity was significantly reduced after 48 h of exposure to FLG at concentrations >30 μg mL^{-1}. In contrast, the GOs significant reduced mitochondrial activity after 24 h of exposure at concentrations as low as 3 μg mL^{-1} for GO1 and GO3 (21% and 25% reduction for GO1 and GO3, respectively) and 10 μg mL^{-1} for GO2 (29% reduction for GO2). The study suggested the large lateral dimension of GO3 along with the graphite starting material might make GO3 the most cytotoxic material. FLG and GOs showed no significant reduction in cell proliferation after 24 and 48 h of exposure. FLG and GOs were also found to impair HaCaT cell membrane integrity and morphology, although long term cytotoxicity was minimal at concentrations as low as 0.1 μg mL^{-1}.

The toxicity of graphene and GO nanosheets appear to be largely due to the physical damage caused to cellular membranes; the damage is induced by direct interactions between the cell membrane and the nanomaterial. Protein corona formation (adsorption of proteins onto the nanoparticles) can mitigate these direct interactions and reduce the cytotoxicity.[232–234] Duan *et al*. demonstrated that protein coatings of bovine serum albumin (BSA) can mitigate the cytotoxicity of GO by reducing the interactions with the cell membrane.[233] Another study showed a reduction in cytotoxicity of GO and rGO nanosheets in human lung carcinoma epithelial cells (A549) by adsorbing one of four blood proteins (bovine fibrinogen, BFG; Ig; transferrin, Tf; and BSA) onto the nanomaterials.[234] Each of the four proteins nearly eliminated cell toxicity. However, the authors noted that, in general, the higher the adsorption capacity of the protein to graphene the better the reduction in toxicity effects.

Graphene-based materials have also been shown to promote cell growth and proliferation.[168-170] Ruiz *et al*. reported graphene as a nonspecific enhancer of cellular growth, by increasing cell attachment and proliferation.[235] Graphene synthesized by CVD was also utilized as a cell culture substrate to promote cardiomyogenic differentiation of mesenchymal stem cells (MSCs). Graphene exhibited no cytotoxicity to stem cells and provided a suitable environment for MSC proliferation.[236] Yet another study found pristine and functionalised graphene to cause negligible (>0.2%) hemolysis in red blood cells at relatively high concentrations (75 μg mL^{-1}).[237] A few studies and their conclusions about the toxicity of graphene-based materials are summarized in **Table 2**.

Even fewer studies have investigated the biocompatibility of 2D TMDs. Like graphene, factors including composition, lateral size, phase, concentration, etc. play a role in determining the cytotoxicity of TMDs.[224] Teo *et al*. systematically demonstrated lower toxicity of chemically exfoliated MoS_2, WS_2, and WSe_2 in comparison to GOs and halogenated graphene in A549 cells.[238] WSe_2 showed dose dependent toxicity indicating that the presence of Se has a significant impact on toxicity. The same group studied the cytotoxicity of chemically exfoliated VTe_2, VSe_2, VTe_2, $NbTe_2$, and $TaTe_2$ with A549 cells at varying dosages.[239,240] Similarly, the role of the chalcogen was investigated by performing a study comparing the toxicities of VS_2, VSe_2, and VTe_2.[239] The VS_2 exhibited the lowest cytotoxicity while VSe_2 and VTe_2 showed a similar and higher cytotoxicity. Moreover, VTe_2 exhibited a higher cytotoxicity in comparison to $NbTe_2$ and $TaTe_2$ (mild toxicity) and the ditellurides exhibited a higher cytotoxicity than the disulphide materials (MoS_2 and WS_2). WSe_2 showed a similar cytotoxicity to ditellurides.[240] Appel *et al*. demonstrated low cytotoxicity and genotoxicity of mechanically and CVD grown pristine MoS_2 and WS_2 2D TMDs.[241] The group performed a fluorescence-based live-dead cell assay and a reactive oxygen species (ROS) assay using human epithelial kidney cells (HEK293f) cells to demonstrate low cytotoxicity. Exposing S. typhimurium TA100 bacteria for prolonged periods of time to high concentrations (100 μM mL^{-1}) of the TMDs also showed no significant mutations.

The form and structure of the 2D materials will also have an impact on the biocompatibility. Chng *et al*. chemically exfoliated MoS_2 nanosheets with three different lithium intercalating agents to produce varying nanosheet size distributions.[242] The study concluded that increased exfoliation produced a stronger cytotoxic effect on the cells. The authors attributed this correlation to the increased surface

area and quantity of defects resulting from extended exfoliation. Chen *et al*. compared the cytotoxicity of CVD grown MoS_2 and MoS_2 microparticles in multiple human cell types.[243] Their research revealed a high cell viability for atomically thin (2D) MoS_2 films as well as larger microparticles. The phase of the TMD can also affect the biocompatibility. For example, Yuan el al. concluded that chemically exfoliated (Ce-WS_2, 1T phase) showed higher levels of cellular uptake, oxidative stress, lipid peroxidation, membrane damage, and inhibition of photosynthesis in algae (chlorella vulgaris) in comparison with annealed exfoliated WS_2 (Ae-WS_2, 2H phase).[244] They attributed the differences to higher electron conductivity and higher separation efficiency of electrons and holes in the 1T phase. This consequently translates to higher photooxidation/reduction activity and a greater ability to generate ROS under visible light radiation.

TMDs can also be functionalized to improve biocompatibility; however, the influence that the functionalization would have on the optical and electronic properties remains less clear. Yin *et al*. decorated MoS_2 nanosheets with chitosan (CS) to improve biocompatibility.[245] The MoS_2 nanosheets were synthesized via a high-throughput, low cost method using a modified oleum treatment exfoliation process. The MoS_2-CS (4-6 nm in thickness, 80 nm lateral size) was used for photothermal DOX delivery to suppress tumor growth in nude mice. Cell viability tests of human epithelial carcinoma (KB) and pancreatic carcinoma (Panc-1) cell lines exposed to MoS_2 and MoS_2-CS revealed that the latter is more biocompatible, as indicated by an enhanced cell viability. Low hemolytic activity toward red blood cells was also demonstrated by the MoS_2-CS nanosheets. Poly(ethylene glycol) (PEG) functionalization has also been shown to improve biocompatibility.[246,247] Hao *et al.* studied the long term *in vivo* biodistribution, excretion, and toxicology of PEGylated MS_2 TMD (M= Mo, W, Ti) nanosheets.[247] The TMDs were synthesized using a high-temperature solution-phase method and ultrasonicated to obtain small single-layer nanosheets. The hydrodynamic diameters determined via DLS were approximately 91, 72, and 102 nm for MoS_2-PEG, WS_2-PEG, and TiS_2-PEG, respectively. *In vitro* toxicity studies toward mouse macrophage (Raw 264.7), human renal epithelial cell (293 T), and mouse breast cancer (4T1) cell lines were performed using the MTT assay. After 24 h of incubation, no statistically significant cytotoxicity was observed for the three PEGylated 2D TMDs, even at concentrations as high as 200 μg mL^{-1}. ROS experiments with dihydroethidine (DHE) also showed no increase in intracellular ROS generation. An *in vivo* biodistribution study in Balb/c mice showed accumulation mostly in RES organs such as the liver and spleen one day post-injection. MoS_2-PEG was excreted almost completely after 30 days, while WS_2-PEG and TiS_2-PEG were still retained in the RES organs in large amounts. Not surprisingly, the metabolic rate of MoS_2-PEG was found to be greater when compared to WS_2-PEG and TiS_2-PEG. Finally, *in vivo* toxicology studies using a haematology assay and histology examination on blood collected from the mice at 1, 7, 30, and 60 days after intravenous injection revealed no obvious long term toxicity caused by any of the PEGylated TMDs.[247] Guan *et al*. reported a method to effectively perform sonication-assisted exfoliation of single-layer MoS_2 using water as the solvent and BSA as an exfoliating agent.[248] The cell viability of MoS_2-BSA was assessed along with other polymer-absorbed MoS_2 nanosheets. It was found that fibroblast cells exposed to MoS_2-BSA nanosheets had a higher cell viability when compared to cells exposed to poly(acrylic acid)-modified MoS_2 nanosheets and polyvinylpyrrolidone-modified MoS_2 nanosheets. A few toxicology studies of TMDs and BN 2D materials and their conclusions are summarized in **Table 3.**

The cytotoxicity of black phosphorus was investigated by Latiff *et al*.[249] Specifically, the WST-8 and MTT cytotoxicity assays were used to study the viability of A549 cells. It was reported that the BP shows dose-dependent toxicity in the concentration range from ~3 μg mL^{-1} to 25 μg mL^{-1}, with cell viabilities of 92% and 82% according to the WST-8 and MTT assays, respectively. However, after 24 hours of incubation at a concentration of 50 μg mL^{-1} the cell viability was 48% and 34% according to the WST-8 and MTT assays, respectively. The size-dependant biocompatibility of BP sheets was investigated by Zhang et al.[250] Cytotoxicity was found to vary with size and concentration. The smallest flakes (~275 nm) showed mild cytotoxicity in comparison with larger flakes (~1100 nm) when cell viability was tested on 293 T cells. The latter showed 100% cell death after 24 h at a concentration of 6.25 μg mL^{-1}. The cell membrane integrity was disrupted by the larger BP flakes.

Similarly, Xiong *et al*. assessed the cytotoxicity of BP against two strains of bacteria: gram-negative *Escherichia coli (E. coli)* and gram-positive *Bacillus subtilis (B. subtilis)*.[251] The bacterial toxicity was examined by monitoring the bacterial growth curve and colony counting. The bactericidal mechanisms were investigated: the intracellular ROS production was detected by fluorescence microscopy and flow cytometry and the bacterial cell membrane damage was assessed by SEM imaging. The study indicated a dose and time dependent toxicity of BP to both the strains. It was also found that after 6 h, BP showed higher toxicity towards *E. Coli* than towards *B. Subtilis.* However, this was reversed at 12 h. The reversal was attributed to the cell membrane self-healing of *E. Coli*. Research done by the same group reported that BP caused ROS-induced bacterial toxicity which, coupled with the sharp edges of the nanosheets acting like knives to disrupt the membrane, led to cell death. The maximum bactericidal efficiency of BP towards *E. Coli* and *B. Subtilis* was 91.65% and 99.69% respectively.

5 Conclusions

The unique electronic, optical, and excitonic properties of quantum materials have created new research directions in biosensing and bio-imaging. The preliminary performance of these materials for sensing, drug delivery, theranostics, and others is quite exciting and impressive. However, despite the tremendous volume of research dedicated to the discovery of new quantum materials for biological applications, the follow-on toxicology studies are lacking. Numerous case studies exist that showcase the negative and

sometimes dire consequences of deploying technologies and materials without first detailing their interactions with biology and the environment. Thus, the purpose of this highlight is to encourage that toxicological investigations be performed in parallel, such that environmental and biological interactions can be incorporated into the material design process and considered as a separate and critical performance attribute.

This work explored a variety of quantum materials and highlighted the properties that make them unique. Great progress has been made in 2D material research since the discovery of graphene and the field has expanded to include multiple new materials such as TMDs, TMOs, black phosphorus, h-BN, etc. The unique electronic properties of 2D materials has made it an emerging contender in the design of the next generation, state-of-the-art biosensors.[34,150,248] With the scale-up and widespread manufacturing of 2D materials bound to happen in the near future, it is important to be proactive in comprehensively understanding the short and long term toxicological and ecological impacts of these materials. The dissolution mechanism of these materials in the environment should be thoroughly understood to mitigate environmental contamination risks. This has become more pertinent since some of the recently discovered 2D materials such as BP have shown high environmental instability.[249]

It is apparent from the above discussion on toxicology that no status quo exists in the screening of 2D materials. Each researcher is left to their own devices in coming up with the appropriate tests and methods to evaluate toxicology. Major strides should be taken to standardize the testing and establish protocol(s) for evaluating these important materials. The *in vitro* toxicity of different 2D materials varies with the choice of cell lines and therefore toxicity studies should involve the use of multiple cells exploring all possible routes of exposure.[246,250] There is also a significant lack of *in vivo* studies validating the forecasted outcomes from the *in vitro* studies; these whole animal studies would provide deeper insights into the effects of systemic exposure. Similarly, the long term biodistribution and bioaccumulation effects of 2D materials must also be elucidated in detail. It is becoming increasingly clear that a generalization of toxicity of these materials should be avoided as toxicity of new materials is dependent on specific applications and development that define the downstream exposure to humans, animals, and the environment.[220,221]

Furthermore, it is important to broaden research on how the 2D material characteristics of size, concentration, number of layers, manufacturing method, etc. affect the toxicology of each of these materials. The toxicity mechanism of each of these materials based on these properties must be fully understood and mapped into a library. This could pave the way for the development of computational tools to predict toxicology behavior of newer 2D materials entering the library. The groundwork laid by Nel *et al.*[253] that describes high throughput toxicology prediction of nanomaterials can be translated over to 2D materials. They suggest that using mechanism-based high-throughput screening *in vitro* enables predictions of physicochemical properties of nanomaterials, these are used to forecast pathology or disease outcomes *in vivo*. Subsequent *in vivo* results are used to validate and improve the *in vitro* screening. High throughput screening aims to develop compositional and combinatorial nanomaterial libraries which can be used to predict *in vivo* injury outcomes using hazard rankings and structure-activity relationships. The library can be expanded to perform mechanism-based toxicology screening. This calls for an integrated model approach where cell lines of interest are investigated before moving to *in vivo* models.

The field of 2D materials is exciting and advancing at an accelerating pace. A balance must be struck between material discovery and risk assessment to ensure sustainable development in this field. In the long run, this balance will help expedite adoption and integration of these materials into new technological devices, increase public acceptance, and shape appropriate legislation and regulations. We conclude by urging our community to continue inventing new materials and probing the underlying physics to gain deeper insights that enable technological advancements, but to also look ahead to the future which requires that material design interfaces with society and the environment in a manner that promotes well-being for all.

Table 2 Recent toxicology studies on graphene-based materials

Reference	Material System	Typical sizes	Results
Zhang *et al*.[255]	Ultrasmall GO	50 nm	Excellent biocompatibility, lower cytotoxicity and higher cellular uptake compared to random large GO sheets
Mittal et al.[256]	GO, thermally reduced GO (TRGO), chemically reduced GO (CRGO)	GO (0.2 - 0.6 µm) TRGO (50 - 250 nm) CRGO (100 - 400 nm)	Graphene oxide derivatives significantly internalize and induce oxidative stress mediated cytotoxicity to human lung cells BEAS-2B and A549
Sasidharan *et al*.[257]	Graphene (hydrophobic) and carboxyl functionalized graphene (hydrophillic)	Not available	Hydrophobic graphene accumulates on cell membranes of Vero cells causing intracellular to ROS stress leading to apoptosis. Hydrophilic graphene is internalized by the cell, allowing normal functioning.
Akhavan *et al*.[258]	Graphene nanosheets deposited in stainless steel substrates in the form of graphene nanowalls (GONW)	Not available	Bacterial cell membranes were damaged by contact with sharp edges of the nanowalls. GONW reduced with hydrazine had higher toxicity towards E.coli bacteria.
Horváth *et al*.[259]	GO, rGO	100 nm – 5 µm	Mild acute cytotoxic action on both epithelial and macrophage cells. ROS generation upon GO exposure may contribute to short-term cytotoxicity
Kryuchkova *et al*.[260]	GO nanoflake	2000 nm	Acutely toxic to P. caudatum cells
Nguyen *et al*.[261]	GO	600 nm	No toxicity against human intestinal bacteria and mild cytotoxic action on Caco-2 cells after 24 h of exposure.
Wu *et al*.[262]	GO	<100 nm	GO had low cytotoxicity, did not induce cell apoptosis or change cell cycle of myeloma cells. GO did not affect antitumor activity of doxorubicin
Chang *et al*.[263]	GO	780 nm (large), 160 nm (small)	No obvious cytotoxicity to A 549 cells, can cause does- dependent oxidative stress at and induce slight loss of cell viability at high concentration. Has favorable cell growth on GO film. Larger GO sheets had better compatibility
Li *et al*.[264]	Graphene	500-1000 nm	Depleted mitochondrial membrane potential, increased ROS, triggered apoptosis

Table 3 Recent studies on toxicology of MoS_2 and other 2D materials

Author	Material	Size	Results
Wang *et al* [265]	MoS_2 (chemically exfoliation: lithium intercalation). PF87-MoS_2 (liquid phase exfoliation: ultrasonication in Pluronic PF87 DI water).	506.3 ± 11.8 nm 72 ± 0.8 nm (hydrodynamic)	In vitro studies showed MoS_2 and PF87-MoS_2 show no cytotoxicity in myeloid (THP-1) and human bronchial epithelial (BEAS-2B) cell lines (>80% viability up to 50 µg mL^{-1}). Aggregated MoS_2 showed strong proinflammatory and profibrogenic response in vitro. In vivo study in mice showed that neither of the MoS_2 2D materials induces acute lung inflammation
Shah *et al*.[266]	MoS_2 (liquid phase exfoliation).	2-3 layer thickness	Cell viability measurement using sulforhodamine B (SRB) assay of RAMEC and PC12 cells showed no significant drop in percentage of cell viability at concentrations as high as 100 µm mL^{-1}. Cell proliferation studies showed no obvious cell death upon incubation with MoS_2 nanosheets.

Moore *et al*.[267]	MoS_2 (liquid phase exfoliation).	lateral size: 50 nm, 117 nm, 177 nm	The varying MoS_2 flake sizes did not induce toxicity in cell lines meant to mimic potential routes of exposure (inhalation A549; ingestion, AGS;monocyte, THP-1) at concentration as 1 μm mL^{-1}. Inflammatory response of cells was attributed to a combination of endotoxin contamination during synthesis, MoS_2 nanomaterials themselves and stabilizing surfactant
Kurapati *et al*.[268]	MoS_2 (chemically exfoliation: lithium intercalation). f-MoS_2 (functionalized with 2-iodacetamide).	Lateral size: 50-500 nm	HeLa and human monocyte-derived macrophage (hMDM) cell viability was not affected at high concentrations (100 μm mL^{-1}). RAW 264.7 macrophage viability reduced to about 20% for f-MoS_2.
Pandit *et al*.[269]	MoS_2 (chemically exfoliated: lithium intercalation) with thiol ligands of varying charge and hydrophobicity.	Monolayers, no lateral size provided	MTT assay of HeLa cells showed low cellular toxicity of functionalized chemically exfoliated MoS_2
Liu *et al*. [270]	MoS_2 (bottom up: one step solvothermal decomposition of ammonium tetraethimolybdate) modified with glutathione (GSH)	Nanodots (<10nm)	GSH functionalization along with small size allowed for efficient body clearance in mice. In vitro cytotoxicity (MTT assay) study showed no significant inhibition of cellular viability after 24h incubation of 4TI murine breast cancer cells with MoS_2-GSH
Wang *et al*. [271]	MoS_2 (bottom up: hydrothermal method)	Thickness: 5 layers -3.25 nm, Lateral size 150 nm	MoS_2 thin films supported the attachment, spreading and maintenance of self-renewing and stemness of neural stem cells (NSCs) and enabled differentiation of NSCs towards neurons and neuroglial cells. Cell viability evaluated via live-dead staining assays showed no significant change in cell viability on exposure to the 2D thin films
Wang *et al*. [272]	MoS_2 (chemical exfoliation: lithium intercalation followed by forced hydration)	Thickness: ~1.2 nm, Lateral size: ~ 250 nm	chemically exfoliated MoS_2 is not toxic to murine macrophages and human lung epithelial cells at doses up to 80 μg mL^{-1}
Corazzari *et al*.[273]	MoS_2 WS_2	361 ± 6 nm 390 ± 5 nm (hydrodynamic)	Lactate dehydrogenase (LDH) release measurement by A549 cells showed no significant toxicity effect from WS_2 even at high doses. MoS_2 induced significant increase in extracellular LDH only at high dose (50/cm^2)
Liu *et al*. [246]	PEG-MoS_2 (chemical exfoliation: lithium intercalation) functionalized with lipoic acid conjugated PEG	Lateral size: ~120 nm thickness: ~ 1nm	MTT assay of Hela cells at 24, 48 and 72 h incubation showed high cell survival rate even under the highest concentration of 160 μm mL^{-1}. PEG- MoS_2 showed slightly improved cell viability at >24 h incubation in comparison with plain MoS_2. (90% in comparison with 80% and 70% respectively for 2- and 3-day assay)
McManus *et al*.[274]	Graphene MoS_2 WS_2 h-BN	Lateral size: ~ 50-350 nm	Cell viability tests using a modified (LDH) assay of human alveolar epithelial (A549; lung) and human keratinocytes (HaCaT; skin) cells when exposed for 24 hours with different 2D material water based inks (graphene, MoS_2,WS_2, and h-BN showed no significant difference in cell viability even at high doses of 100 μg mL^{-1}.
Liu *et al*.[275]	MoS_2 BN	441.2 nm 472.7 nm	Cytotoxicity study on human hepatoma HepG2 cells showed decreased cell viability at 30 μg mL^{-1} on exposure to both materials. MoS_2 and BN nanomaterials also induced an increase in intracellular ROS (>2 μg mL^{-1}) and compromised membrane integrity (>8 μg mL^{-1} for MoS_2 and >2 μg mL^{-1} for BN).Low exposure concentrations (0.2- 2 μg mL^{-1}) could increase plasma membrane fluidity and inhibit transmembrane ATP binding cassette (ABC) efflux transporter activity

Conflicts of interest

There are no conflicts to declare.

Acknowledgements

The authors acknowledge Mr. Michael Tran and Ms. Shiljashree Vijay for helpful discussions. M.M.K. and M.D.G acknowledge support from NASA under grant number 80NSSC18K1508 and the Army Research Office under grant number W911NF-18-1-0412. S.T. acknowledges support from Department of Energy (DOE) under grant number DE-SC0020653.

References

1 K. S. Novoselov, A. K. Geim, S. V Morozov, D. Jiang, Y. Zhang, S. V Dubonos, I. V Grigorieva and A. A. Firsov, *Electric Field Effect in Atomically Thin Carbon Films*, Kluwer, 2000, vol. 404.

2 M. W. Roberts, C. B. Clemons, J. P. Wilber, G. W. Young, A. Buldum and D. D. Quinn, *J. Nanotechnol.*, , DOI:10.1155/2010/868492.

3 H. Zeng and X. Cui, *Chem. Soc. Rev.*, 2015, 44, 2629–2642.

4 Z. Xia, Q. Huang and S. Guo, *FlatChem*, 2019, 17, 100129.

5 H. Cao, Z. Yu and P. Lu, *Superlattices Microstruct.*, 2015, **86**, 501–507.

6 J. Wang, F. Ma and M. Sun, *RSC Adv.*, 2017, 7, 16801–16822.

7 L. Kou, C. Chen and S. C. Smith, *J. Phys. Chem. Lett.*, 2015, 6, 2794–2805.

8 N. Briggs, S. Subramanian, Z. Lin, X. Li, X. Zhang, K. Zhang, K. Xiao, D. Geohegan, R. Wallace, L.-Q. Chen, M. Terrones, A. Ebrahimi, S. Das, J. Redwing, C. Hinkle, K. Momeni, A. van Duin, V. Crespi, S. Kar and J. A. Robinson, *2D Mater.*, 2019, **6**, 022001.

9 M. D. Stoller, S. Park, Y. Zhu, J. An and R. S. Ruoff, , DOI:10.1021/nl802558y.

10 C. Lee, X. Wei, J. W. Kysar and J. Hone, *Science (80-.).*, 2008, **321**, 385–388.

11 R. R. Nair, P. Blake, A. N. Grigorenko, K. S. Novoselov, T. J. Booth, T. Stauber, N. M. R. Peres and A. K. Geim, *Science (80-.).*, 2008, **320**, 1308.

12 A. A. Balandin, S. Ghosh, W. Bao, I. Calizo, D. Teweldebrhan, F. Miao and C. N. Lau, , DOI:10.1021/nl0731872.

13 A. K. Geim and K. S. Novoselov, *Nat. Mater.*, 2007, **6**, 183–191.

14 W. Choi, N. Choudhary, G. H. Han, J. Park, D. Akinwande and Y. H. Lee, *Mater. Today*, 2017, 20, 116–130.

15 K. Kalantar-zadeh, J. Z. Ou, T. Daeneke, A. Mitchell, T. Sasaki and M. S. Fuhrer, *Appl. Mater. Today*, 2016, 5, 73–89.

16 K. Zhang, Y. Feng, F. Wang, Z. Yang and J. Wang, *J. Mater. Chem. C*, 2017, 5, 11992–12022.

17 J. C. Lei, X. Zhang and Z. Zhou, *Front. Phys.*, 2015, 10, 276–286.

18 M. Zhao, Y. Huang, Y. Peng, Z. Huang, Q. Ma and H. Zhang, *Chem. Soc. Rev.*, 2018, 47, 6267–6295.

19 M. Pumera and Z. Sofer, *Adv. Mater.*, 2017, **29**, 1605299.

20 K. Liu, M. Lihter, A. Sarathy, S. Caneva, H. Qiu, D. Deiana, V. Tileli, D. T. L. Alexander, S. Hofmann, D. Dumcenco, A. Kis, J. P. Leburton and A. Radenovic, *Nano Lett.*, 2017, **17**, 4223–4230.

21 P. Li, Y. Wen, X. He, Q. Zhang, C. Xia, Z. M. Yu, S. A. Yang, Z. Zhu, H. N. Alshareef and X. X. Zhang, *Nat. Commun.*, 2017, **8**, 1–8.

22 L. Du, X. Li, W. Lou, G. Sullivan, K. Chang, J. Kono and R. R. Du, *Nat. Commun.*, 2017, **8**, 1–8.

23 V. Tran, R. Soklaski, Y. Liang and L. Yang, *Phys. Rev. B - Condens. Matter Mater. Phys.*, 2014, **89**, 235319.

24 Y. Wang, X. Huang, D. Wu, R. Zhuo, E. Wu, C. Jia, Z. Shi, T. Xu, Y. Tian and X. Li, *J. Mater. Chem. C*, 2018, **6**, 4861–4865.

25 B. Liu, M. Köpf, A. N. Abbas, X. Wang, Q. Guo, Y. Jia, F. Xia, R. Weihrich, F. Bachhuber, F. Pielnhofer, H. Wang, R. Dhall, S. B. Cronin, M. Ge, X. Fang, T. Nilges and C. Zhou, *Adv. Mater.*, 2015, **27**, 4423–4429.

26 O. Lopez-Sanchez, D. Lembke, M. Kayci, A. Radenovic and A. Kis, *Nat. Nanotechnol.*, 2013, **8**, 497–501.

27 Z. Sofer, D. Sedmidubský, Š. Huber, J. Luxa, D. Bouša, C. Boothroyd and M. Pumera, *Angew. Chemie Int. Ed.*, 2016, **55**, 3382–3386.

28 B. Jiang, Z. Yang, X. Liu, Y. Liu and L. Liao, *Nano Today*, 2019, 25, 122–134.

29 D. S. Kim, T. C. Ozawa, K. Fukuda, S. Ohshima, I. Nakai and T. Sasaki, *Chem. Mater.*, 2011, **23**, 2700–2702.

30 B. Zhan, C. Li, J. Yang, G. Jenkins, W. Huang and X. Dong, *Small*, 2014, **10**, n/a-n/a.

31 D. Sarkar, W. Liu, X. Xie, A. C. Anselmo, S. Mitragotri and K. Banerjee, *ACS Nano*, 2014, **8**, 3992–4003.

32 S. Kim, J. Nah, I. Jo, D. Shahrjerdi, L. Colombo, Z. Yao, E. Tutuc and S. K. Banerjee, *Appl. Phys. Lett.*, 2009, **94**, 062107.

33 Q. Xi, D. M. Zhou, Y. Y. Kan, J. Ge, Z. K. Wu, R. Q. Yu and J. H. Jiang, *Anal. Chem.*, 2014, **86**, 1361–1365.

34 J. Peña-Bahamonde, H. N. Nguyen, S. K. Fanourakis and D. F. Rodrigues, *J. Nanobiotechnology*, 2018, 16, 1–17.

35 W. Wen, Y. Song, X. Yan, C. Zhu, D. Du, S. Wang, A. M. Asiri and Y. Lin, *Mater. Today*, 2018, 21, 164–177.

36 L. Lin, H. Peng and Z. Liu, *Nat. Mater.*, 2019, 18, 520–524.

37 A. S. Mayorov, R. V. Gorbachev, S. V. Morozov, L. Britnell, R. Jalil, L. A. Ponomarenko, P. Blake, K. S. Novoselov, K. Watanabe, T. Taniguchi and A. K. Geim, *Nano Lett.*, 2011, **11**, 2396–2399.

38 K. Liu and J. Wu, *J. Mater. Res.*, 2016, **31**, 832–844.

39 J. S. Bunch, S. S. Verbridge, J. S. Alden, A. M. Van Der Zande, J. M. Parpia, H. G. Craighead and P. L. McEuen, *Nano Lett.*, 2008, **8**, 2458–2462.

40 R. R. Nair, W. Ren, R. Jalil, I. Riaz, V. G. Kravets, L. Britnell, P. Blake, F. Schedin, A. S. Mayorov, S. Yuan, M. I. Katsnelson, H. M. Cheng, W. Strupinski, L. G. Bulusheva, A. V. Okotrub, I. V. Grigorieva, A. N. Grigorenko, K. S. Novoselov and A. K. Geim, *Small*, 2010, **6**, 2877–2884.

41 D. C. Elias, R. R. Nair, T. M. G. Mohiuddin, S. V. Morozov, P. Blake, M. P. Halsall, A. C. Ferrari, D. W. Boukhvalov, M. I. Katsnelson, A. K. Geim and K. S. Novoselov, *Science (80-.).*, 2009, **323**, 610–613.

42 S. Bae, H. Kim, Y. Lee, X. Xu, J. S. Park, Y. Zheng, J. Balakrishnan, T. Lei, H. Ri Kim, Y. Il Song, Y. J. Kim, K. S. Kim, B. Özyilmaz, J. H. Ahn, B. H. Hong and S. Iijima, *Nat. Nanotechnol.*, 2010, **5**, 574–578.

43 F. A. Armstrong, H. A. O. Hill and N. J. Walton, *Acc. Chem. Res.*, 1988, **21**, 407–413.

44 Y. L. Yao and K. K. Shiu, *Electroanalysis*, 2008, **20**, 1542–1548.

45 C. Léger and P. Bertrand, *Chem. Rev.*, 2008, 108, 2379–2438.

46 L. Zhang, Q. Zhang and J. Li, *Adv. Funct. Mater.*, 2007, **17**,

1958–1965.
47 Y. Shao, J. Wang, H. Wu, J. Liu, I. A. Aksay and Y. Lin, *Electroanalysis*, 2010, 22, 1027–1036.
48 X. Duan, C. Wang, A. Pan, R. Yu and X. Duan, *Chem. Soc. Rev.*, 2015, 44, 8859–8876.
49 A. Splendiani, L. Sun, Y. Zhang, T. Li, J. Kim, C.-Y. Chim, G. Galli and F. Wang, , DOI:10.1021/nl903868w.
50 K. F. Mak, C. Lee, J. Hone, J. Shan and T. F. Heinz, *Phys. Rev. Lett.*, 2010, **105**, 136805.
51 R. Ganatra and Q. Zhang, *ACS Nano*, 2014, 8, 4074–4099.
52 M. Chhowalla, D. Jena and H. Zhang, *Nat. Rev. Mater.*, 2016, 1, 1–15.
53 W. Zhao, Z. Ghorannevis, L. Chu, M. Toh, C. Kloc, P. H. Tan and G. Eda, *ACS Nano*, 2013, **7**, 791–797.
54 A. Chernikov, T. C. Berkelbach, H. M. Hill, A. Rigosi, Y. Li, O. B. Aslan, D. R. Reichman, M. S. Hybertsen and T. F. Heinz, , DOI:10.1103/PhysRevLett.113.076802.
55 D. Sun, Y. Rao, G. A. Reider, G. Chen, Y. You, L. Brézin, A. R. Harutyunyan and T. F. Heinz, *Nano Lett.*, 2014, **14**, 5625–5629.
56 G. Wang, A. Chernikov, M. M. Glazov, T. F. Heinz, X. Marie, T. Amand and B. Urbaszek, *Rev. Mod. Phys.*, 2018, **90**, 021001.
57 C. Jin, E. C. Regan, A. Yan, M. Iqbal Bakti Utama, D. Wang, S. Zhao, Y. Qin, S. Yang, Z. Zheng, S. Shi, K. Watanabe, T. Taniguchi, S. Tongay, A. Zettl and F. Wang, *Nature*, 2019, 567, 76–80.
58 X. Xu, W. Yao, D. Xiao and T. F. Heinz, *Nat. Phys.*, 2014, 10, 343–350.
59 G. Wang, C. Robert, A. Suslu, B. Chen, S. Yang, S. Alamdari, I. C. Gerber, T. Amand, X. Marie, S. Tongay and B. Urbaszek, *Nat. Commun.*, 2015, **6**, 1–7.
60 K. F. Mak, K. L. McGill, J. Park and P. L. McEuen, *Science (80-.).*, 2014, **344**, 1489–1492.
61 S. Tongay, H. Sahin, C. Ko, A. Luce, W. Fan, K. Liu, J. Zhou, Y. S. Huang, C. H. Ho, J. Yan, D. F. Ogletree, S. Aloni, J. Ji, S. Li, J. Li, F. M. Peeters and J. Wu, *Nat. Commun.*, 2014, **5**, 1–6.
62 A. Ambrosi, Z. Sofer and M. Pumera, *Chem. Commun.*, 2015, **51**, 8450–8453.
63 C. Backes, N. C. Berner, X. Chen, P. Lafargue, P. LaPlace, M. Freeley, G. S. Duesberg, J. N. Coleman and A. R. McDonald, *Angew. Chemie Int. Ed.*, 2015, **54**, 2638–2642.
64 J. K. Dash, L. Chen, P. H. Dinolfo, T. M. Lu and G. C. Wang, *J. Phys. Chem. C*, 2015, **119**, 19763–19771.
65 D. Voiry, A. Mohite and M. Chhowalla, *Chem. Soc. Rev.*, 2015, 44, 2702–2712.
66 M. Chhowalla, H. S. Shin, G. Eda, L. J. Li, K. P. Loh and H. Zhang, *Nat. Chem.*, 2013, 5, 263–275.
67 A. Splendiani, L. Sun, Y. Zhang, T. Li, J. Kim, C.-Y. Chim, G. Galli and F. Wang, , DOI:10.1021/nl903868w.
68 Q. Ouyang, S. Zeng, L. Jiang, J. Qu, X. Q. Dinh, J. Qian, S. He, P. Coquet and K. T. Yong, *J. Phys. Chem. C*, 2017, **121**, 6282–6289.
69 X. Liu, H. L. Shuai, Y. J. Liu and K. J. Huang, *Sensors Actuators, B Chem.*, 2016, **235**, 603–613.
70 Z. Sun, T. Liao, Y. Dou, S. Min Hwang, M.-S. Park, L. Jiang, J. Ho Kim and S. Xue Dou, *Nat. Commun.*, , DOI:10.1038/ncomms4813.
71 J. Mannhart and D. G. Schlom, *Science (80-.).*, 2010, 327, 1607–1611.
72 H. Y. Hwang, Y. Iwasa, M. Kawasaki, B. Keimer, N. Nagaosa and Y. Tokura, *Nat. Mater.*, 2012, 11, 103–113.
73 M. Osada and T. Sasaki, *J. Mater. Chem.*, 2009, **19**, 2503–2511.
74 T. Sasaki and M. Watanabe, *J. Phys. Chem. B*, 1997, **101**, 10159–10161.
75 S. Balendhran, S. Walia, M. Alsaif, E. P. Nguyen, J. Z. Ou, S. Zhuiykov, S. Sriram, M. Bhaskaran and K. Kalantar-Zadeh, *ACS Nano*, 2013, **7**, 9753–9760.
76 Y. Wang, K. Jiang, J. Zhu, L. Zhang and H. Lin, *Chem. Commun.*, 2015, **51**, 12748–12751.
77 Z. Zhao, H. Fan, G. Zhou, H. Bai, H. Liang, R. Wang, X. Zhang and W. Tan, *J. Am. Chem. Soc.*, 2014, **136**, 11220–11223.
78 M. Naguib, V. N. Mochalin, M. W. Barsoum and Y. Gogotsi, *Adv. Mater.*, 2014, **26**, 992–1005.
79 U. Yorulmaz, A. Özden, N. K. Perkgöz, F. Ay and C. Sevik, *Nanotechnology*, 2016, **27**, 335702.
80 X. H. Wang and Y. C. Zhou, *Corros. Sci.*, 2003, **45**, 891–907.
81 F. Wang, C. Yang and Y. Tang, *Artic. J. Electrochem. Soc.*, , DOI:10.1149/2.0371501jes.
82 H. C. J. Zhou and S. Kitagawa, *Chem. Soc. Rev.*, 2014, 43, 5415–5418.
83 X. W. Yan, M. Joharian, M. Naghiloo, R. Rasuli, M. L. Hu and A. Morsali, *Mater. Lett.*, 2019, **252**, 325–328.
84 B. Lalmi, H. Oughaddou, H. Enriquez, A. Kara, Ś. Vizzini, B. Ealet and B. Aufray, *Appl. Phys. Lett.*, 2010, **97**, 223109.
85 L. Tao, E. Cinquanta, D. Chiappe, C. Grazianetti, M. Fanciulli, M. Dubey, A. Molle and D. Akinwande, , DOI:10.1038/NNANO.2014.325.
86 W. J. Ong, L. L. Tan, Y. H. Ng, S. T. Yong and S. P. Chai, *Chem. Rev.*, 2016, 116, 7159–7329.
87 J. Zhang, Y. Chen and X. Wang, *Energy Environ. Sci.*, 2015, **8**, 3092–3108.
88 J. Wang, F. Ma, W. Liang and M. Sun, *Mater. Today Phys.*, 2017, 2, 6–34.
89 H. Liu, Y. Du, Y. Deng and P. D. Ye, *Chem. Soc. Rev.*, 2015, 44, 2732–2743.
90 V. Eswaraiah, Q. Zeng, Y. Long and Z. Liu, *Small*, 2016, **12**, 3480–3502.
91 D. Singh, S. K. Gupta, Y. Sonvane and I. Lukačević, *J. Mater. Chem. C*, 2016, **4**, 6386–6390.
92 S. Zhang, W. Zhou, Y. Ma, J. Ji, B. Cai, S. A. Yang, Z. Zhu, Z. Chen and H. Zeng, *Nano Lett.*, 2017, **17**, 3434–3440.
93 S. Zhang, Z. Yan, Y. Li, Z. Chen and H. Zeng, *Angew. Chemie - Int. Ed.*, 2015, **54**, 3112–3115.
94 C. C. Mayorga-Martinez, R. Gusmão, Z. Sofer and M. Pumera, *Angew. Chemie - Int. Ed.*, 2019, **58**, 134–138.
95 J. D. Caldwell, I. Aharonovich, G. Cassabois, J. H. Edgar, B. Gil and D. N. Basov, *Nat. Rev. Mater.*, 2019, 4, 552–567.
96 W. Lei, D. Portehault, D. Liu, S. Qin and Y. Chen, *Nat. Commun.*, 2013, **4**, 1–7.
97 J. Wu, B. Wang, Y. Wei, R. Yang and M. Dresselhaus, *Mater. Res. Lett.*, 2013, **1**, 200–206.
98 G. Ciofani, S. Danti, G. G. Genchi, B. Mazzolai and V. Mattoli, *Small*, 2013, **9**, 1672–1685.
99 Q. Weng, B. Wang, X. Wang, N. Hanagata, X. Li, D. Liu, X. Wang, X. Jiang, Y. Bando and D. Golberg, *ACS Nano*, 2014, **8**, 6123–6130.
100 L. Li, Y. Yu, G. J. Ye, Q. Ge, X. Ou, H. Wu, D. Feng, X. H. Chen and Y. Zhang, *Nat. Nanotechnol. |*, , DOI:10.1038/NNANO.2014.35.
101 W. Zhang, T. Huynh, P. Xiu, B. Zhou, C. Ye, B. Luan and R. Zhou, *Carbon N. Y.*, 2015, **94**, 895–902.
102 Y. B. Pottathara, Y. Grohens, V. Kokol, N. Kalarikkal and S.

Thomas, in *Nanomaterials Synthesis: Design, Fabrication and Applications*, Elsevier, 2019, pp. 1–25.
103 E. Gao, S. Z. Lin, Z. Qin, M. J. Buehler, X. Q. Feng and Z. Xu, *J. Mech. Phys. Solids*, 2018, **115**, 248–262.
104 H. Li, J. Wu, Z. Yin and H. Zhang, *Acc. Chem. Res.*, 2014, **47**, 1067–1075.
105 H. Li, Z. Yin, Q. He, H. Li, X. Huang, G. Lu, D. W. H. Fam, A. I. Y. Tok, Q. Zhang and H. Zhang, *Small*, 2012, **8**, 63–67.
106 D. J. Late, S. N. Shirodkar, U. V. Waghmare, V. P. Dravid and C. N. R. Rao, *ChemPhysChem*, 2014, **15**, 1592–1598.
107 A. Castellanos-Gomez, L. Vicarelli, E. Prada, J. O. Island, K. L. Narasimha-Acharya, S. I. Blanter, D. J. Groenendijk, M. Buscema, G. A. Steele, J. V Alvarez, H. W. Zandbergen, J. J. Palacios and H. S. J. van der Zant, *2D Mater.*, 2014, **1**, 025001.
108 M. Buscema, D. J. Groenendijk, S. I. Blanter, G. A. Steele, H. S. J. Van Der Zant and A. Castellanos-Gomez, *Nano Lett*, 2014, **14**, 3352.
109 P. Ares, F. Aguilar-Galindo, D. Rodríguez-San-Miguel, D. A. Aldave, S. Díaz-Tendero, M. Alcamí, F. Martín, J. Gómez-Herrero and F. Zamora, *Adv. Mater.*, 2016, **28**, 6332–6336.
110 N. Alem, R. Erni, C. Kisielowski, M. D. Rossell, W. Gannett and A. Zettl, *Phys. Rev. B - Condens. Matter Mater. Phys.*, 2009, **80**, 155425.
111 A. Ciesielski and P. Samorì, *Chem. Soc. Rev.*, 2014, 43, 381–398.
112 C. Tan and H. Zhang, *Nat. Commun.*, , DOI:10.1038/ncomms8873.
113 K. R. Paton, E. Varrla, C. Backes, R. J. Smith, U. Khan, A. O'Neill, C. Boland, M. Lotya, O. M. Istrate, P. King, T. Higgins, S. Barwich, P. May, P. Puczkarski, I. Ahmed, M. Moebius, H. Pettersson, E. Long, J. Coelho, S. E. O'Brien, E. K. McGuire, B. M. Sanchez, G. S. Duesberg, N. McEvoy, T. J. Pennycook, C. Downing, A. Crossley, V. Nicolosi and J. N. Coleman, *Nat. Mater.*, 2014, **13**, 624–630.
114 E. Varrla, C. Backes, K. R. Paton, A. Harvey, Z. Gholamvand, J. McCauley and J. N. Coleman, *Chem. Mater.*, 2015, **27**, 1129–1139.
115 Y. Hernandez, V. Nicolosi, M. Lotya, F. M. Blighe, Z. Sun, S. De, I. T. Mcgovern, B. Holland, M. Byrne, Y. Gun'ko, J. Boland, P. Niraj, G. Duesberg, S. Krishnamurti, R. Goodhue, J. Hutchison, V. Scardaci, A. C. Ferrari and J. N. Coleman, *High yield production of graphene by liquid phase exfoliation of graphite*, .
116 J. N. Coleman, M. Lotya, A. O'Neill, S. D. Bergin, P. J. King, U. Khan, K. Young, A. Gaucher, S. De, R. J. Smith, I. V. Shvets, S. K. Arora, G. Stanton, H. Y. Kim, K. Lee, G. T. Kim, G. S. Duesberg, T. Hallam, J. J. Boland, J. J. Wang, J. F. Donegan, J. C. Grunlan, G. Moriarty, A. Shmeliov, R. J. Nicholls, J. M. Perkins, E. M. Grieveson, K. Theuwissen, D. W. McComb, P. D. Nellist and V. Nicolosi, *Science (80-.).*, 2011, **331**, 568–571.
117 S. Vadukumpully, J. Paul and S. Valiyaveettil, *Carbon N. Y.*, 2009, **47**, 3288–3294.
118 T. Hasan, F. Torrisi, Z. Sun, D. Popa, V. Nicolosi, G. Privitera, F. Bonaccorso and A. C. Ferrari, *Phys. status solidi*, 2010, **247**, 2953–2957.
119 P. May, U. Khan, J. M. Hughes and J. N. Coleman, *J. Phys. Chem. C*, 2012, **116**, 11393–11400.
120 A. B. Bourlinos, V. Georgakilas, R. Zboril, T. A. Steriotis, A. K. Stubos and C. Trapalis, *Solid State Commun.*, 2009, **149**, 2172–2176.
121 L. Liu, Z. Shen, M. Yi, X. Zhang and S. Ma, *RSC Adv.*, 2014, **4**, 36464–36470.
122 Z. Cai, B. Liu, X. Zou and H. M. Cheng, *Chem. Rev.*, 2018, 118, 6091–6133.
123 J. Yu, J. Li, W. Zhang and H. Chang, *Chem. Sci.*, 2015, **6**, 6705–6716.
124 X. Zhang, H. Nan, S. Xiao, X. Wan, X. Gu, A. Du, Z. Ni and K. (Ken) Ostrikov, *Nat. Commun.*, 2019, **10**, 1–10.
125 J. You, M. D. Hossain and Z. Luo, *Nano Converg.*, 2018, 5, 1–13.
126 Y. Zhang, L. Zhang and C. Zhou, *Acc. Chem. Res.*, 2013, **46**, 2329–2339.
127 Q. Ji, Y. Zheng, Y. Zhang and Z. Liu, *Chem. Soc. Rev.*, 2015, 44, 2587–2602.
128 N. Liu, L. Fu, B. Dai, K. Yan, X. Liu, R. Zhao, Y. Zhang and Z. Liu, *Nano Lett.*, 2011, **11**, 297–303.
129 Y. Gong, S. Lei, G. Ye, B. Li, Y. He, K. Keyshar, X. Zhang, Q. Wang, J. Lou, Z. Liu, R. Vajtai, W. Zhou and P. M. Ajayan, , DOI:10.1021/acs.nanolett.5b02423.
130 M. W. Chen, D. Ovchinnikov, S. Lazar, M. Pizzochero, M. B. Whitwick, A. Surrente, M. Baranowski, O. L. Sanchez, P. Gillet, P. Plochocka, O. V. Yazyev and A. Kis, *ACS Nano*, 2017, **11**, 6355–6361.
131 Y. Zhang, T. R. Chang, B. Zhou, Y. T. Cui, H. Yan, Z. Liu, F. Schmitt, J. Lee, R. Moore, Y. Chen, H. Lin, H. T. Jeng, S. K. Mo, Z. Hussain, A. Bansil and Z. X. Shen, *Nat. Nanotechnol.*, 2014, **9**, 111–115.
132 R. Yue, Y. Nie, L. A. Walsh, R. Addou, C. Liang, N. Lu, A. T. Barton, H. Zhu, Z. Che, D. Barrera, L. Cheng, P.-R. Cha, Y. J. Chabal, J. W. P. Hsu, J. Kim, M. J. Kim, L. Colombo, R. M. Wallace, K. Cho and C. L. Hinkle, *2D Mater.*, 2017, **4**, 045019.
133 E. Moreau, F. J. Ferrer, D. Vignaud, S. Godey and X. Wallart, *Phys. status solidi*, 2010, **207**, 300–303.
134 H. J. Liu, L. Jiao and L. Xie, , DOI:10.1088/1367-2630/17/5/053023.
135 A. Khosravi, R. Addou, C. M. Smyth, R. Yue, C. R. Cormier, J. Kim, C. L. Hinkle and R. M. Wallace, *APL Mater.*, 2018, **6**, 026603.
136 L. L. Fan, S. Chen, Y. F. Wu, F. H. Chen, W. S. Chu, X. Chen, C. W. Zou and Z. Y. Wu, *Appl. Phys. Lett.*, 2013, **103**, 131914.
137 B. Jalan, P. Moetakef and S. Stemmer, *Appl. Phys. Lett.*, 2009, **95**, 032906.
138 H. C. Diaz, Y. Ma, R. Chaghi and M. Batzill, *Appl. Phys. Lett.*, 2016, **108**, 191606.
139 R. I. Walton, *Chem. Soc. Rev.*, 2002, 31, 230–238.
140 Z. Zhuang, Q. Peng and Y. Li, *Chem. Soc. Rev.*, 2011, 40, 5492–5513.
141 X. Guo, Y. Wang, F. Wu, Y. Ni and S. Kokot, *Analyst*, 2015, **140**, 1119–1126.
142 N. Chaudhary, M. Khanuja, Abid and S. S. Islam, *Sensors Actuators, A Phys.*, 2018, **277**, 190–198.
143 Z. Wang, C. Schliehe, T. Wang, Y. Nagaoka, Y. C. Cao, W. A. Bassett, H. Wu, H. Fan and H. Weller, *J. Am. Chem. Soc.*, 2011, **133**, 14484–14487.
144 Z. Wu, Y. Li, J. Liu, Z. Lu, H. Zhang and B. Yang, *Angew. Chemie Int. Ed.*, 2014, **53**, 12196–12200.
145 P. Simon, L. Bahrig, I. A. Baburin, P. Formanek, F. Röder, J. Sickmann, S. G. Hickey, A. Eychmüller, H. Lichte, R. Kniep and E. Rosseeva, *Adv. Mater.*, 2014, **26**, 3042–3049.
146 K. Selvarani, A. Prabhakaran, P. Arumugam, S. Berchmans

and P. Nayak, *Microchim. Acta*, 2018, **185**, 1–8.
147 N. Dontschuk, A. Stacey, A. Tadich, K. J. Rietwyk, A. Schenk, M. T. Edmonds, O. Shimoni, C. I. Pakes, S. Prawer and J. Cervenka, *Nat. Commun.*, 2015, **6**, 1–7.
148 S. Afsahi, M. B. Lerner, J. M. Goldstein, J. Lee, X. Tang, D. A. Bagarozzi, D. Pan, L. Locascio, A. Walker, F. Barron and B. R. Goldsmith, *Biosens. Bioelectron.*, 2018, **100**, 85–88.
149 S. Kaushik, U. K. Tiwari, S. S. Pal and R. K. Sinha, *Biosens. Bioelectron.*, 2019, **126**, 501–509.
150 H. Huang, S. Su, N. Wu, H. Wan, S. Wan, H. Bi and L. Sun, *Front. Chem.*, 2019, 7.
151 C. I. L. Justino, A. R. Gomes, A. C. Freitas, A. C. Duarte and T. A. P. Rocha-Santos, *TrAC - Trends Anal. Chem.*, 2017, 91, 53–66.
152 J. Lin, X. Chen and P. Huang, *Adv. Drug Deliv. Rev.*, 2016, 105, 242–254.
153 C. Zhao, L. Xing, J. Xiang, L. Cui, J. Jiao, H. Sai, Z. Li and F. Li, *Particuology*, 2014, **17**, 66–73.
154 H. W. Kim, H. W. Yoon, B. M. Yoo, J. S. Park, K. L. Gleason, B. D. Freeman and H. B. Park, *Chem. Commun.*, 2014, **50**, 13563–13566.
155 E. L. Albert, C. A. Che Abdullah and Y. Shiroshaki, *Results Phys.*, 2018, **11**, 944–950.
156 L. Fei, S. H. Yoo, R. A. R. Villamayor, B. P. Williams, S. Y. Gong, S. Park, K. Shin and Y. L. Joo, *ACS Appl. Mater. Interfaces*, 2017, **9**, 9738–9746.
157 H. P. Cong, X. C. Ren, P. Wang and S. H. Yu, *Sci. Rep.*, 2012, **2**, 1–6.
158 E. Y. Jang, J. Carretero-González, A. Choi, W. J. Kim, M. E. Kozlov, T. Kim, T. J. Kang, S. J. Baek, D. W. Kim, Y. W. Park, R. H. Baughman and Y. H. Kim, *Nanotechnology*, 2012, **23**, 235601.
159 W. S. Hummers and R. E. Offeman, *J. Am. Chem. Soc.*, 1958, **80**, 1339.
160 X. Zhu, L. Sun, Y. Chen, Z. Ye, Z. Shen and G. Li, *Biosens. Bioelectron.*, 2013, **47**, 32–37.
161 W. Putzbach and N. Ronkainen, *Sensors*, 2013, **13**, 4811–4840.
162 H. H. Nguyen, S. H. Lee, U. J. Lee, C. D. Fermin and M. Kim, *Materials (Basel).*, 2019, 12.
163 A. Weltin, J. Kieninger and G. A. Urban, *Anal. Bioanal. Chem.*, 2016, 408, 4503–4521.
164 P. Das, M. Das, S. R. Chinnadayyala, I. M. Singha and P. Goswami, *Biosens. Bioelectron.*, 2016, 79, 386–397.
165 S. K. Krishnan, E. Singh, P. Singh, M. Meyyappan and H. S. Nalwa, *RSC Adv.*, 2019, 9, 8778–8781.
166 J. H. Lee, S. J. Park and J. W. Choi, *Nanomaterials*, 2019, 9.
167 M. Qi, Y. Zhang, C. Cao, Y. Lu and G. Liu, *RSC Adv.*, 2016, **6**, 39180–39187.
168 M. N. Omar, A. B. Salleh, H. N. Lim and A. Ahmad Tajudin, *Anal. Biochem.*, 2016, **509**, 135–141.
169 B. Jiang, K. Zhou, C. Wang, Q. Sun, G. Yin, Z. Tai, K. Wilson, J. Zhao and L. Zhang, *Sensors Actuators, B Chem.*, 2018, **254**, 1033–1039.
170 Y. Liu, D. Yu, C. Zeng, Z. Miao and L. Dai, *Langmuir*, 2010, **26**, 6158–6160.
171 V. Georgakilas, M. Otyepka, A. B. Bourlinos, V. Chandra, N. Kim, K. C. Kemp, P. Hobza, R. Zboril and K. S. Kim, *Chem. Rev.*, 2012, **112**, 6156–6214.
172 V. Georgakilas, J. N. Tiwari, K. C. Kemp, J. A. Perman, A. B. Bourlinos, K. S. Kim and R. Zboril, *Chem. Rev.*, 2016, 116, 5464–5519.
173 A. M. Lopez Marzo, C. C. Mayorga-Martinez and M. Pumera, , DOI:10.1016/j.bios.2019.111980.
174 V. Crivianu-Gaita and M. Thompson, *Biosens. Bioelectron.*, 2016, 85, 32–45.
175 S. Mao, K. Yu, J. Chang, D. A. Steeber, L. E. Ocola and J. Chen, *Sci. Rep.*, 2013, **3**, 1–6.
176 J. H. Lee, Y. K. Choi, H. J. Kim, R. H. Scheicher and J. H. Cho, *J. Phys. Chem. C*, 2013, **117**, 13435–13441.
177 F. Ortmann, W. G. Schmidt and F. Bechstedt, *Phys. Rev. Lett.*, 2005, **95**, 186101.
178 Z. Hao, Y. Zhu, X. Wang, P. G. Rotti, C. Dimarco, S. R. Tyler, X. Zhao, J. F. Engelhardt, J. Hone and Q. Lin, , DOI:10.1021/acsami.7b07684.
179 S. Xu, J. Zhan, B. Man, S. Jiang, W. Yue, S. Gao, C. Guo, H. Liu, Z. Li, J. Wang and Y. Zhou, *Nat. Commun.*, 2017, **8**, 1–10.
180 H. Gu, H. Tang, P. Xiong and Z. Zhou, *Nanomaterials*, 2019, 9.
181 X. Zhu, Y. Liu, P. Li, Z. Nie and J. Li, *Analyst*, 2016, **141**, 4541–4553.
182 L. A. Ponomarenko, F. Schedin, M. I. Katsnelson, R. Yang, E. W. Hill, K. S. Novoselov and A. K. Geim, *Science (80-.).*, 2008, **320**, 356–358.
183 Y. Du and S. Guo, *Nanoscale*, 2016, 8, 2532–2543.
184 Y. Li, Y. Zhao, H. Cheng, Y. Hu, G. Shi, L. Dai and L. Qu, *J. Am. Chem. Soc.*, 2012, **134**, 15–18.
185 D. Qu, M. Zheng, L. Zhang, H. Zhao, Z. Xie, X. Jing, R. E. Haddad, H. Fan and Z. Sun, *Sci. Rep.*, 2014, **4**, 1–11.
186 H. Bian, Q. Wang, S. Yang, C. Yan, H. Wang, L. Liang, Z. Jin, G. Wang and S. Liu, *J. Mater. Chem. A*, 2019, **7**, 5740–5747.
187 H. Wang, R. Revia, K. Wang, R. J. Kant, Q. Mu, Z. Gai, K. Hong and M. Zhang, *Adv. Mater.*, , DOI:10.1002/adma.201605416.
188 S. Li, Y. Li, J. Cao, J. Zhu, L. Fan and X. Li, *Anal. Chem.*, 2014, **86**, 10201–10207.
189 Z. Li, D. Wang, M. Xu, J. Wang, X. Hu, S. Anwar, A. C. Tedesco, P. C. Morais and H. Bi, *J. Mater. Chem. B*, 2020, **8**, 2598–2606.
190 M. K. Kumawat, R. Srivastava, M. Thakur and R. B. Gurung, *ACS Sustain. Chem. Eng.*, 2017, **5**, 1382–1391.
191 D. Qu, M. Zheng, J. Li, Z. Xie and Z. Sun, *Light Sci. Appl.*, 2015, **4**, e364–e364.
192 H. Chen, F. Liu, Z. Lei, L. Ma and Z. Wang, *RSC Adv.*, 2015, **5**, 84980–84987.
193 D. W. Lee, J. Lee, I. Y. Sohn, B. Y. Kim, Y. M. Son, H. Bark, J. Jung, M. Choi, T. H. Kim, C. Lee and N. E. Lee, *Nano Res.*, 2015, **8**, 2340–2350.
194 S. Dutta, A. Dutta Chowdhury, S. Biswas, E. Y. Park, N. Agnihotri, A. De and S. De, *Biochem. Eng. J.*, 2018, **140**, 130–139.
195 F. Li, H. Yin, Y. Chen, S. Wang, J. Li, Y. Zhang, C. Li and S. Ai, *J. Colloid Interface Sci.*, 2020, **561**, 348–357.
196 A. Khataee, M. Haddad Irani-nezhad, J. Hassanzadeh and S. Woo Joo, *J. Colloid Interface Sci.*, 2018, **515**, 39–49.
197 J.-K. Yang, H.-R. Lee, I.-J. Hwang, H.-I. Kim, D. Yim and J.-H. Kim, *Adv. Healthc. Mater.*, 2018, **7**, 1701496.
198 X. Ran, F. Pu, Z. Wang, J. Ren and X. Qu, *Anal. Chim. Acta*, 2019, **1056**, 1–6.
199 J. Ge, R. Cai, X. Chen, Q. Wu, L. Zhang, Y. Jiang, C. Cui, S. Wan and W. Tan, *Talanta*, 2019, **195**, 40–45.
200 P. Yang, G. Cai, X. Wang and Y. Pei, *IEEE Trans. Electron Devices*, 2019, **66**, 3554–3559.

201 M. L. Yola and N. Atar, *Appl. Surf. Sci.*, 2018, **458**, 648–655.
202 L. Zhou, C. Liu, Z. Sun, H. Mao, L. Zhang, X. Yu, J. Zhao and X. Chen, *Biosens. Bioelectron.*, 2019, **137**, 140–147.
203 A. J. Storm, J. H. Chen, H. W. Zandbergen and C. Dekker, *Phys. Rev. E - Stat. Nonlinear, Soft Matter Phys.*, 2005, **71**, 051903.
204 U. F. Keyser, B. N. Koeleman, S. Van Dorp, D. Krapf, R. M. M. Smeets, S. G. Lemay, N. H. Dekker and C. Dekker, *Nat. Phys.*, 2006, **2**, 473–477.
205 D. Fologea, M. Gershow, B. Ledden, D. S. McNabb, J. A. Golovchenko and J. Li, *Nano Lett.*, 2005, **5**, 1905–1909.
206 J. Li, D. Stein, C. McMullan, D. Branton, M. J. Aziz and J. A. Golovchenko, *Nature*, 2001, **412**, 166–169.
207 F. Traversi, C. Raillon, S. M. Benameur, K. Liu, S. Khlybov, M. Tosun, D. Krasnozhon, A. Kis and A. Radenovic, *Nat. Nanotechnol.*, 2013, **8**, 939–945.
208 K. Liu, J. Feng, A. Kis and A. Radenovic, *ACS Nano*, 2014, **8**, 2504–2511.
209 S. Garaj, W. Hubbard, A. Reina, J. Kong, D. Branton and J. A. Golovchenko, *Nature*, 2010, **467**, 190–193.
210 G. F. Schneider, S. W. Kowalczyk, V. E. Calado, G. Pandraud, H. W. Zandbergen, L. M. K. Vandersypen and C. Dekker, *Nano Lett.*, 2010, **10**, 3163–3167.
211 J. Luo, S. Jiang, H. Zhang, J. Jiang and X. Liu, *Anal. Chim. Acta*, 2012, **709**, 47–53.
212 Y. Zhang, W. Lei, Q. Wu, X. Xia and Q. Hao, *Microchim. Acta*, 2017, **184**, 3103–3111.
213 A. T. E. Vilian, S. M. Chen, M. A. Ali and F. M. A. Al-Hemaid, *RSC Adv.*, 2014, **4**, 30358–30367.
214 A. Halder, M. Zhang and Q. Chi, *Biosens. Bioelectron.*, 2017, **87**, 764–771.
215 D. Geng, X. Bo and L. Guo, *Sensors Actuators, B Chem.*, 2017, **244**, 131–141.
216 S. Wu, H. Huang, M. Shang, C. Du, Y. Wu and W. Song, *Biosens. Bioelectron.*, 2017, **92**, 646–653.
217 J. Wu and L. Yin, *ACS Appl. Mater. Interfaces*, 2011, **3**, 4354–4362.
218 S. S.-M. J. S.-C. Ranganethan, *J. Sens. Sci. Technol.*, 2017, **26**, 379–385.
219 S. Garaj, S. Liu, J. A. Golovchenko and D. Branton, *Proc. Natl. Acad. Sci. U. S. A.*, 2013, **110**, 12192–12196.
220 G. F. Schneider, Q. Xu, S. Hage, S. Luik, J. N. H. Spoor, S. Malladi, H. Zandbergen and C. Dekker, *Nat. Commun.*, 2013, **4**, 1–7.
221 A. Merlo, V. R. S. S. Mokkapati, S. Pandit and I. Mijakovic, *Biomater. Sci.*, 2018, 6, 2298–2311.
222 N. C. D. Nath, T. Debnath, M. Nurunnabi and E.-K. Kim, in *Biomedical Applications of Graphene and 2D Nanomaterials*, Elsevier, 2019, pp. 165–186.
223 Kenry and C. T. Lim, *ChemNanoMat*, 2017, **3**, 5–16.
224 L. M. Guiney, X. Wang, T. Xia, A. E. Nel and M. C. Hersam, *ACS Nano*, 2018, 12, 6360–6377.
225 A. Bianco, *Angew. Chemie - Int. Ed.*, 2013, 52, 4986–4997.
226 V. C. Sanchez, A. Jachak, R. H. Hurt and A. B. Kane, *Chem. Res. Toxicol.*, 2012, 25, 15–34.
227 T. Nezakati, B. G. Cousins and A. M. Seifalian, *Arch. Toxicol.*, 2014, 88, 1987–2012.
228 A. B. Seabra, A. J. Paula, R. De Lima, O. L. Alves and N. Durán, *Chem. Res. Toxicol.*, 2014, 27, 159–168.
229 Y. Chong, Y. Ma, H. Shen, X. Tu, X. Zhou, J. Xu, J. Dai, S. Fan and Z. Zhang, *Biomaterials*, 2014, **35**, 5041–5048.
230 D. Wang, L. Zhu, J. F. Chen and L. Dai, *Nanoscale*, 2015, **7**, 9894–9901.
231 M. Pelin, L. Fusco, V. León, C. Martín, A. Criado, S. Sosa, E. Vázquez, A. Tubaro and M. Prato, *Sci. Rep.*, 2017, **7**, 1–12.
232 W. Hu, C. Peng, M. Lv, X. Li, Y. Zhang, N. Chen, C. Fan and Q. Huang, *ACS Nano*, 2011, **5**, 3693–3700.
233 G. Duan, S. G. Kang, X. Tian, J. A. Garate, L. Zhao, C. Ge and R. Zhou, *Nanoscale*, 2015, **7**, 15214–15224.
234 Y. Chong, C. Ge, Z. Yang, J. A. Garate, Z. Gu, J. K. Weber, J. Liu and R. Zhou, *ACS Nano*, 2015, **9**, 5713–5724.
235 O. N. Ruiz, K. A. S. Fernando, B. Wang, N. A. Brown, P. G. Luo, N. D. McNamara, M. Vangsness, Y. P. Sun and C. E. Bunker, *ACS Nano*, 2011, **5**, 8100–8107.
236 J. Park, S. Park, S. Ryu, S. H. Bhang, J. Kim, J.-K. Yoon, Y. H. Park, S.-P. Cho, S. Lee, B. H. Hong and B.-S. Kim, *Adv. Healthc. Mater.*, 2014, **3**, 176–181.
237 A. Sasidharan, L. S. Panchakarla, A. R. Sadanandan, A. Ashokan, P. Chandran, C. M. Girish, D. Menon, S. V. Nair, C. N. R. Rao and M. Koyakutty, *Small*, 2012, **8**, 1251–1263.
238 W. Z. Teo, E. L. K. Chng, Z. Sofer and M. Pumera, *Chem. - A Eur. J.*, 2014, **20**, 9627–9632.
239 N. M. Latiff, Z. Sofer, A. C. Fisher and M. Pumera, *Chem. - A Eur. J.*, 2017, **23**, 684–690.
240 H. L. Chia, N. M. Latiff, Z. Sofer and M. Pumera, *Chem. - A Eur. J.*, 2018, **24**, 206–211.
241 J. H. Appel, D. O. Li, J. D. Podlevsky, A. Debnath, A. A. Green, Q. H. Wang and J. Chae, *ACS Biomater. Sci. Eng.*, 2016, **2**, 361–367.
242 E. L. K. Chng, Z. Sofer and M. Pumera, *Nanoscale*, 2014, **6**, 14412–14418.
243 W. Chen, W. Qi, W. Lu, N. R. Chaudhury, J. Yuan, L. Qin and J. Lou, *Small*, 2018, **14**, 1702600.
244 P. Yuan, Q. Zhou and X. Hu, *Environ. Sci. Technol.*, 2018, **52**, 13543–13552.
245 W. Yin, L. Yan, J. Yu, G. Tian, L. Zhou, X. Zheng, X. Zhang, Y. Yong, J. Li, Z. Gu and Y. Zhao, *ACS Nano*, 2014, **8**, 6922–6933.
246 T. Liu, C. Wang, X. Gu, H. Gong, L. Cheng, X. Shi, L. Feng, B. Sun and Z. Liu, *Adv. Mater.*, 2014, **26**, 3433–3440.
247 J. Hao, G. Song, T. Liu, X. Yi, K. Yang, L. Cheng and Z. Liu, *Adv. Sci.*, , DOI:10.1002/advs.201600160.
248 G. Guan, S. Zhang, S. Liu, Y. Cai, M. Low, C. P. Teng, I. Y. Phang, Y. Cheng, K. L. Duei, B. M. Srinivasan, Y. Zheng, Y. W. Zhang and M. Y. Han, *J. Am. Chem. Soc.*, 2015, **137**, 6152–6155.
249 N. M. Latiff, W. Z. Teo, Z. Sofer, A. C. Fisher and M. Pumera, *Chem. – A Eur. J.*, 2015, **21**, 13991–13995.
250 X. Zhang, Z. Zhang, S. Zhang, D. Li, W. Ma, C. Ma, F. Wu, Q. Zhao, Q. Yan and B. Xing, *Small*, 2017, **13**, 1701210.
251 Z. Xiong, X. Zhang, S. Zhang, L. Lei, W. Ma, D. Li, W. Wang, Q. Zhao and B. Xing, *Ecotoxicol. Environ. Saf.*, 2018, **161**, 507–514.
252 P. Bollella, G. Fusco, C. Tortolini, G. Sanzò, G. Favero, L. Gorton and R. Antiochia, *Biosens. Bioelectron.*, 2017, 89, 152–166.
253 A. Nel, T. Xia, H. Meng, X. Wang, S. Lin, Z. Ji and H. Zhang, *Acc. Chem. Res.*, 2013, **46**, 607–621.
254 S. Mullick Chowdhury, G. Lalwani, K. Zhang, J. Y. Yang, K. Neville and B. Sitharaman, *Biomaterials*, 2013, **34**, 283–293.
255 H. Zhang, C. Peng, J. Yang, M. Lv, R. Liu, D. He, C. Fan and Q. Huang, *ACS Appl. Mater. Interfaces*, 2013, **5**, 1761–1767.
256 S. Mittal, V. Kumar, N. Dhiman, L. K. S. Chauhan, R. Pasricha

and A. K. Pandey, *Sci. Rep.*, 2016, **6**, 1–16.
257 A. Sasidharan, L. S. Panchakarla, P. Chandran, D. Menon, S. Nair, C. N. R. Rao and M. Koyakutty, *Nanoscale*, 2011, **3**, 2461–2464.
258 O. Akhavan and E. Ghaderi, *ACS Nano*, 2010, **4**, 5731–5736.
259 L. Horváth, A. Magrez, M. Burghard, K. Kern, L. Forró and B. Schwaller, *Carbon N. Y.*, 2013, **64**, 45–60.
260 M. Kryuchkova, A. Danilushkina, Y. Lvov and R. Fakhrullin, *Environ. Sci. Nano*, 2016, **3**, 442–452.
261 T. H. D. Nguyen, M. Lin and A. Mustapha, *J. Food Prot.*, 2015, **78**, 996–1002.
262 S. Wu, X. Zhao, Z. Cui, C. Zhao, Y. Wang, L. Du and Y. Li, *Int. J. Nanomedicine*, 2014, **9**, 1413–1421.
263 Y. Chang, S. T. Yang, J. H. Liu, E. Dong, Y. Wang, A. Cao, Y. Liu and H. Wang, *Toxicol. Lett.*, 2011, **200**, 201–210.
264 Y. Li, Y. Liu, Y. Fu, T. Wei, L. Le Guyader, G. Gao, R. S. Liu, Y. Z. Chang and C. Chen, *Biomaterials*, 2012, **33**, 402–411.
265 X. Wang, N. D. Mansukhani, L. M. Guiney, Z. Ji, C. H. Chang, M. Wang, Y.-P. Liao, T.-B. Song, B. Sun, R. Li, T. Xia, M. C. Hersam and A. E. Nel, *Small*, 2015, **11**, 5079–5087.
266 P. Shah, T. N. Narayanan, C.-Z. Li and S. Alwarappan, *Nanotechnology*, 2015, **26**, 315102.
267 C. Moore, D. Movia, R. J. Smith, D. Hanlon, F. Lebre, E. C. Lavelle, H. J. Byrne, J. N. Coleman, Y. Volkov and J. McIntyre, *2D Mater.*, 2017, **4**, 025065.
268 R. Kurapati, L. Muzi, A. P. R. de Garibay, J. Russier, D. Voiry, I. A. Vacchi, M. Chhowalla and A. Bianco, *Adv. Funct. Mater.*, 2017, **27**, 1605176.
269 S. Pandit, S. Karunakaran, S. K. Boda, B. Basu and M. De, *ACS Appl. Mater. Interfaces*, 2016, **8**, 31567–31573.
270 T. Liu, Y. Chao, M. Gao, C. Liang, Q. Chen, G. Song, L. Cheng and Z. Liu, , DOI:10.1007/s12274-016-1183-x.
271 S. Wang, J. Qiu, W. Guo, X. Yu, J. Nie, J. Zhang, X. Zhang, Z. Liu, X. Mou, L. Li and H. Liu, *Adv. Biosyst.*, 2017, **1**, 1600042.
272 Z. Wang, A. Von Dem Bussche, Y. Qiu, T. M. Valentin, K. Gion, A. B. Kane and R. H. Hurt, *Environ. Sci. Technol.*, 2016, **50**, 7208–7217.
273 I. Corazzari, F. A. Deorsola, G. Gulino, E. Aldieri, S. Bensaid, F. Turci and D. Fino, *J. Nanoparticle Res.*, 2014, **16**, 1–14.
274 D. McManus, S. Vranic, F. Withers, V. Sanchez-Romaguera, M. Macucci, H. Yang, R. Sorrentino, K. Parvez, S. K. Son, G. Iannaccone, K. Kostarelos, G. Fiori and C. Casiraghi, *Nat. Nanotechnol.*, 2017, **12**, 343–350.
275 S. Liu, Z. Shen, B. Wu, Y. Yu, H. Hou, X. X. Zhang and H. Q. Ren, *Environ. Sci. Technol.*, 2017, **51**, 10834–10842.

Table of Contents Entry:

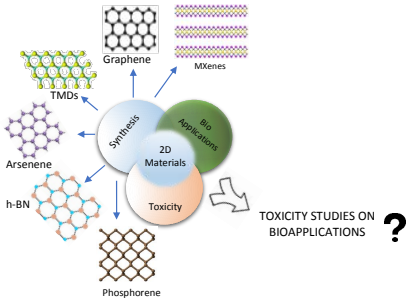

Biological applications of novel quantum materials require an intimate interface between the material and biology. Thus, toxicological investigations should be performed in parallel such that biological interactions can be considered as a separate and critical performance attribute.